Journal of Theoretical Biology 458 (2018) 148–155

Contents lists available at ScienceDirect

Journal of Theoretical Biology

journal homepage: www.elsevier.com/locate/jtb

Stochastic modeling of tumor progression and immune evasion

Jason T. George[a,b,c,*], Herbert Levine[a,b,d,*]

[a] Center for Theoretical Biological Physics, Rice University, Houston, TX, USA
[b] Department of Bioengineering, Rice University, Houston, TX, USA
[c] Medical Scientist Training Program, Baylor College of Medicine, Houston, TX, USA
[d] Department of Physics and Astronomy, Rice University, Houston, TX, USA

ARTICLE INFO

Article history:
Received 17 May 2018
Revised 16 August 2018
Accepted 11 September 2018
Available online 12 September 2018

MSC:
00-01
99-00

Keywords:
Cancer immunotherapy
Immune evasion
Applied probability
Stochastic processes

ABSTRACT

It is now well-established that the host's adaptive immune system plays an important role in identifying and eliminating cancer cells in much the same way that intracellular pathogens are cleared during an adaptive immune response to infection. From a therapeutic standpoint, the adaptive immune system is unique in that it can co-evolve alongside a developing tumor. Tumor acquisition of immune evasive phenotypes, such as class-I MHC down-regulation, remains a major limitation of successful T-cell immunotherapy. Here, we consider a population dynamical model coupling tumor and adaptive immune compartments in order to study the dynamics and survival of an evolving threat when faced with adaptive immune pressure. We demonstrate that predicted optimal growth strategies depend on whether or not the threat may acquire an immune-evasive phenotype as well as the mode of immune detection. We parameterize adaptive immune functioning by T-cell turnover and repertoire diversity and predict that decreases in the latter quantity which occur in advanced age may substantially affect the ability to recognize, and therefore control, an immune evasive threat like cancer. This framework recapitulates general features of age-dependent AML incidence, thereby providing a probable association between cancer frequency and adaptive immune functioning. Lastly, we quantify therapeutic efficacy of adjuvant immunotherapeutic strategies, and predict their benefits and limitations with regard to handling immune evasion. Our model generates survival behavior consistent with known growth-dependent characteristics, and serves as a first attempt at modeling stochastic cancer evolution alongside an adaptive immune compartment.

1. Introduction

The lack of successful treatment options that lead to durable remission outcomes still remains an ongoing challenge for curing many malignancies. However, there have been significant advances made most recently in targeted and immune therapeutic strategies (Couzin-Frankel, 2013). It is now well-established that the cytotoxic (CD8+) T-cell compartment of the human adaptive immune system plays an integral role in immunoediting, and tumor progression therefore necessarily requires successful evasion of adaptive immune surveillance (Dunn et al., 2002; Fridman et al., 2011). More recently, immunotherapy has become one of the most promising areas of cancer research and treatment. This general approach encompasses strategies aimed at enhancing the patient's immune system via tumor antigen vaccines (Fritsch et al., 2014; Hellmann and Snyder, 2017; Ott et al., 2017; Sahin et al., 2017), immune checkpoint inhibition (Alsaab et al., 2017; Leach et al., 1996), and introduction of tumor-specific immune cells, as is the case in chimeric antigen receptor (CAR) T-cell therapy (Martin et al., 2016; Sadelain et al., 2017; Wang and Rivière, 2016).

Despite these advances, tumors may acquire treatment-resistant clones during disease progression (Iwasa et al., 2006), thus limiting treatment efficacy. Cancer cells exploit a variety of strategies that facilitate CD8+ T-cell immune evasion (Bronte and Mocellin, 2009), including up-regulation of immune inhibitory genes like programmed death-ligand 1 (PD-L1) and human leukocyte antigen (HLA)-G (Driessens et al., 2009; Herbst et al., 2014; Lin and Yan, 2015; Sheu and Shih, 2010), reduced immunoproteasome expression (Tripathi et al., 2016), and complete evasion of CD8+ recognition via loss of major hisocompatibility class-I (MHC-I) (del Campo et al., 2014; Carretero et al., 2008; Garrido et al., 2016; Straten and Garrido, 2016). Such evasive tactics occur alongside active immunosurveillance by an adaptive T-cell repertoire. Naïve T-cell turnover can, in theory, lead to recognition of a dividing cancer

* Corresponding authors.
E-mail addresses: jason.george@rice.edu (J.T. George), herbert.levine@rice.edu (H. Levine).

https://doi.org/10.1016/j.jtbi.2018.09.012
0022-5193/

cell population prior to acquisition of an immune-evasive phenotype. Previous studies have considered systems-level interactions between the tumor and host adaptive immune system (Andrew et al., 2007; Khailaie et al., 2013; Kirschner and Panetta, 1998; Nani and OÇŞuztöreli, 1994; Sontag, 2017), while a separate effort has gone into understanding the acquisition of drug-resistant subpopulations during clonal evolution (Iwasa et al., 2006; Michor et al., 2004). At present, the temporal dynamics of acquired immune evasion on tumor development under adaptive immune pressure remains uncharacterized. Filling this gap is of fundamental importance to better understand tumor progression. Additionally, an improved quantitative framework for describing the successes, and failures, of adaptive immune targeting of cancer cells would enable more accurate predictions of treatment success rates.

Here, we propose a foundational model of the co-evolution between an adaptive immune system and an evading threat such as cancer whereinaffected cells may be recognized by the immune system, but may also acquire an immune-evasive phenotype. We account for key empirical behaviors, including the growth-threshold conjecture which predicts that initiation of an immune response depends on threat net growth rate instead of absolute threat size (Arias et al., 2015; Grossman and Paul, 1992; Johansen et al., 2008; Pradeu et al., 2013). For threats like cancer which may acquire an immune evasive phenotype, we show that the model supports the experimental observation of 'sneak-through' wherein threats with either large or small net growth rates have a preferential advantage over their intermediate-growth counterparts (Bocharov et al., 2004). We apply this model to study acute myeloid leukemia (AML) incidence as a function of immune turnover and repertoire diversity, and accurately characterize increased incidence as a result of an aging immune system in addition to chronic immunosuppression. We conclude our analysis by quantifying the benefit of certain types of T-cell immunotherapy and predicting treatment-specific advantages based on tumor growth rates and patient immune status.

2. Model development

We conceptualize the dynamics between a foreign threat and the host immune system as a time-continuous birth process, where the state variable, X, represents the total number of cancerous or infected cells. In our model, these cells grow at net rate r per cell until either exceeding a critical size, $M \gg 1$, or until the immune system mounts a response at a (possibly random) population size $X = m$ and time S_1. If recognized, the population undergoes net death at a per-cell rate of $\tilde{r} = d - r$ so that d characterizes per-cell immune system killing rate. We assume d is large enough to handle threats with a variety of growth rates so that $r < d$ always. States 0 and $M+1$ are absorbing. A more precise model would separately track birth and death rates both before and after treatment. We have opted for this simpler form to enable analytic investigations.

2.1. Static threats

Static threats are those unable to acquire an immune evasive phenotype. These dynamics are most appropriate for investigating intracellular microbial pathogens that grow, divide, and infect host cells. In this case the process evolves according to the following transitions:

$$\begin{aligned} t < S_1: &\quad x \to x+1 \text{ at rate } rx \\ t \geq S_1: &\quad x \to x-1 \text{ at rate } \tilde{r}x \end{aligned} \tag{1}$$

2.2. Dynamic threats

Dynamic threats, including cancer, may randomly acquire an immune evasive phenotype that enables its members to avoid immune recognition targeting the initial population. We therefore consider two cell populations: a non-evasive population, X_1, and an immune evasive population, X_2 that broadly represents cells adopting a variety of CD8+ T-cell evasion strategies commonly observed during cancer progression. We assume that immune evasive cells are randomly acquired at rate $\mu \ll 1$ per cell division. Transitions are described by:

$$\begin{aligned} &t < S_1: \\ &\quad (x_1, x_2) \to (x_1, x_2+1) \text{ at rate } \mu r x_1 + r x_2 \\ &\quad (x_1, x_2) \to (x_1+1, x_2) \text{ at rate } (1-\mu) r x_1 \approx r x_1 \\ &t \geq S_1: \\ &\quad (x_1, x_2) \to (x_1, x_2+1) \text{ at rate } \mu r x_1 + r x_2 \\ &\quad (x_1, x_2) \to (x_1-1, x_2) \text{ at rate } [d-(1-\mu)r] x_1 \approx \tilde{r} x_1 \end{aligned} \tag{2}$$

We assume that successful immune responses occur quickly and are not limited at large population sizes for both the static and dynamic cases.

2.3. Detection limit

We assume that immune recognition at size $X_1 = m$ may only occur after the population reaches a lower detection limit, m_0, based either on the population size or the population total net growth rate. We will refer to the former assumption as the ***size threshold*** or ***size-limited*** case ($m_0 = m_c$), and the latter as the ***growth-threshold*** or ***growth-limited*** case ($m_0 = m_0(r)$ such that the total net growth rate first exceeds R), where appropriate. The growth-threshold conjecture is supported by empirical and theoretical observations (Arias et al., 2015; Grossman and Paul, 1992; Johansen et al., 2008; Pradeu et al., 2013; Sontag, 2017). We will argue later that a size-limited model is perhaps most appropriate for modeling CAR T-cell infusions, as CAR T-cell self-activation is engineered directly in this case.

2.4. Recognition mode

In the primary case of interest we model the response of an adaptive immune compartment whose present and future CD8+ T-cell repertoire may contain a T-cell receptor (TCR) capable of recognizing an immune susceptible threat X_1. There is continual opportunity for the sensitive population to be recognized as its growth trajectory exceeds m_0 and continues growing to final size M. We refer to this case hereafter as ***stochastic*** or ***adaptive recognition***. Recognition depends on both the T-cell repertoire and turnover of new T-cell clones. The population at size m_0 evades the current immune repertoire, due in part to a lack of sufficient levels of detectable antigen or recognizing T-cells, with a background escape probability p_b, which we use to represent the clonal diversity of the TCR repertoire (larger p_b implies lower diversity). We model the arrival of a recognizing T-cell clone as a Poisson process with rate k, corresponding to the thymic turnover rate of naïve CD8+ T-cells. It is also convenient to analyze a simpler process wherein a growing threat is (deterministically) recognized at threshold size m_0, which applies for example to innate immune recognition of, or memory reactivation to, a previously encountered threat. We refer to this case as ***deterministic recognition***.

2.5. Mathematical analysis

Here we provide a broad outline of our general strategy, with the primary goal of calculating the probability that a threat either

escapes immune detection, or acquires an evasive phenotype, or is controlled and subsequently cleared by the immune system. Complete derivations are included in the SI. We let E_e denote the event that a threat escapes recognition and exceeds size M with corresponding probability P_e. For dynamic threats, E_μ denotes the event that an immune evader arrives with probability P_μ. All events may be partitioned by: $E_{e,\,\mu} \equiv E_e \cap E_\mu$, $E_{e,\mu^c} \equiv E_e \cap E_\mu^c$, $E_{e^c,\mu} \equiv E_e^c \cap E_\mu$, and $E_{e^c,\mu^c} \equiv E_e^c \cap E_\mu^c$ with corresponding probabilities $P_{e,\,\mu}$, P_{e,μ^c}, $P_{e^c,\mu}$, and P_l (a threat loses if it neither escapes nor acquires an evader, see SI Sec. S5).

P_e is determined by relating the immune turnover and size parameters to recognition probabilities (Section 3.1). This may be obtained by solving for the probability that recognition occurs at size $m \geq m_0$, denoted by $p_r(m;\, m_0)$ (SI Section S3). The calculation of $P_{e^c,\mu}$ is more involved, and so we begin first by evaluating this quantity under deterministic recognition at fixed size m, denoted $P_{e^c,\mu}(m)$. We recall that S_1 denotes type-1 arrival time. If τ_2 is the type-2 arrival time, and $\tilde{S}_1$ the type-1 extinction time, then the probability of interest can be expressed as

$$P_{e^c,\mu}(m) = \mathbb{P}\big(\tau_2 < S_1 \;\big|\; X_1(S_1) = m\big) + \mathbb{P}\big(S_1 \leq \tau_2 < \tilde{S}_1 \;\big|\; X_1(S_1) = m\big), \tag{3}$$

with both terms amenable to exact calculation by conditioning on the exponential inter-arrival times of each birth/death event (SI Section S5.1). The corresponding probability under adaptive recognition with variable detection size, denoted $P_{e^c,\mu}(m_0 \leq m \leq M)$, may be calculated by taking weighted averages of each estimate conditioned on size m recognition via

$$P_{e^c,\mu}(m_0 \leq m \leq M) = \sum_{m=m_0}^{M} P_{e^c,\mu}(m) \cdot p_r(m;\, m_0), \tag{4}$$

provided $m_0 < M$ (SI Section S5.3). In all cases, P_l is calculated indirectly via

$$P_l = 1 - (P_{e^c,\mu} + P_e). \tag{5}$$

We obtain a solution in the adaptive recognition mode by weighting by the distribution of recognition sizes, calculated subsequently.

Under deterministic recognition, we also characterize the mean first time of type-2 arrival conditioned on acquired evasion, given by $T_\mu(m) \equiv \mathbb{E}[\tau_2 | \tau_2 < \tilde{S}_1]$. Using the usual indicator random variable notation

$$I_{[\tau_2 < \tilde{S}_1]} = \begin{cases} 1, & \tau_2 < \tilde{S}_1; \\ 0, & \tau_2 \not< \tilde{S}_1. \end{cases} \tag{6}$$

This quantity may be calculated using the definition of conditional probability

$$T_\mu(m) = \frac{\mathbb{E}[\tau_2 I_{[\tau_2 < \tilde{S}_1]}]}{\mathbb{P}\big(\tau_2 < \tilde{S}_1\big)}, \tag{7}$$

and is derived to first order in μ following a similar strategy for characterizing $P_{e^c,\mu}$, here instead assuming each inter-arrival time is well-characterized by its mean value (SI Section S5.2). This framework permits analytical comparisons between predicted evasion behavior for the various assumptions on detection limit and recognition mode. We apply this framework to study AML, a hematological malignancy, as our model disease due to its low mutation rate, relative immune accessibility, and rapid growth. We compare model predictions to AML incidence data, comparing our theory with the alternative 'multi-stage' theory of cancer incidence (Armitage and Doll, 1954), and conclude by expanding the analysis to predict post-immunotherapy treatment success probabilities.

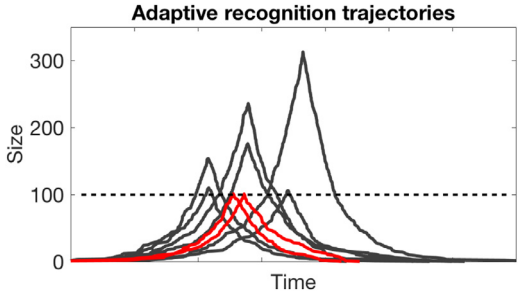

Fig. 1. Dynamics under adaptive immune detection. Stochastic population trajectories obeying Eq. (1) that are ultimately recognized and eliminated. Red trajectories illustrate recognition at detection limit m_0 (dashed line) ($r = 0.1$, $d = 0.2$, $m_0 = 10^2$, $p_b = 0.75$, $k = 0.1$). (For interpretation of the references to color in this figure legend, the reader is referred to the web version of this article).

3. Tumor progression

The following sections present the main findings of our analysis. Full mathematical details are provided in the SI. In an effort to organize subsequent analyses, we subdivide outcomes of the process based on relevant events.

3.1. Adaptive repertoire and detection limit determine escape probability

This section focuses on static threats ($P_\mu = 0$). If recognition is deterministic, then $P_e = 0$ trivially. Adaptive recognition in contrast permits a threat to grow past minimal detection before recognition and subsequent elimination (Fig. 1), as long as $m_0 < M$ (for large simulation trajectories illustrating mean-variance behavior, see Fig. 1 in George and Levine, 2018). In this case a population's survival probability is inversely related to its mean sojourn time on $\{m_0, \ldots, M\}$, given by

$$\Delta t_s(r) \approx \log\big(M/m_0\big) r^{-1}. \tag{8}$$

The probability of recognition at size m is given by

$$p_r(m;\, m_0) \approx \begin{cases} 0, & m < m_0; \\ 1 - p_b e^{-\frac{k}{rm_0}}, & m = m_0; \\ p_b\big(1 - e^{-\frac{k}{rm}}\big)\big(\frac{m_0}{m}\big)^{\frac{k}{r}}, & m_0 < m \leq M. \end{cases} \tag{9}$$

From this formula, we observe that the escape probability up to size $m > m_0$ is

$$p_e(m;\, m_0) = p_b\Big(\frac{m_0}{m}\Big)^{k/r}. \tag{10}$$

It is clear from the above that optimal growth rates of immune evaders balance the size of earliest detection with the amount of time spent under immunosurveillance. Faster growing threats always have higher escape probabilities if detection is size-limited. However, under growth-limited detection the existence of a slow-growth window $r \in (0,\, eR/M)$ enables threats with slow growth rates to increase the likelihood of escape by minimizing surveillance time (Table S1). Thus, growth-limited detection of a static threat demonstrates sneak-through of threats with small growth rates (Arias et al., 2015; Bocharov et al., 2004; Grossman and Paul, 1992; Johansen et al., 2008; Pradeu et al., 2013). Analogously, if $m_c > M$ in the size-limited case, then clearly threats of all growth rates escape detection. Cumulative recognition probabilities, given by $1 - p_e(m;\, m_0)$, are presented for a variety of immune parameters (Fig. 2), indicating the relevance of repertoire diversity and T-cell turnover to tumor recognition.

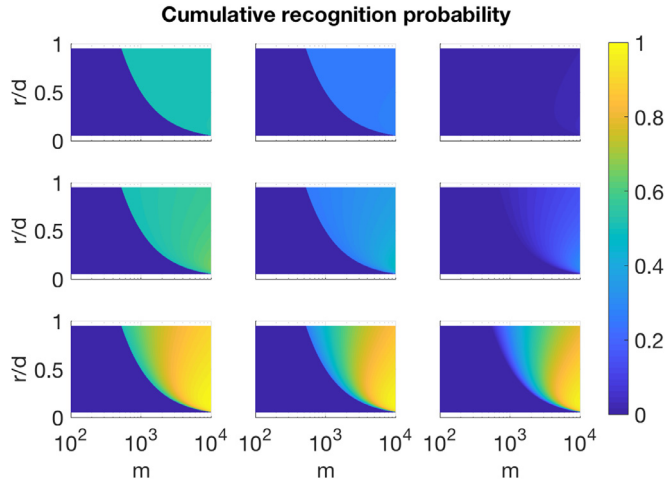

Fig. 2. Growth-limited cumulative recognition. Cumulative recognition probability $1 - p_e(m; m_0)$ as a function of population size m and relative growth rate r/d for various values of immune turnover (rows bottom-to-top: $k = \{10^{-1}, 10^{-2}, 10^{-3}\}$) and repertoire diversity (columns left-to-right: $p_b = \{0.5, 0.75, 1.0\}$) ($d = 0.2$, $R = 10^2$).

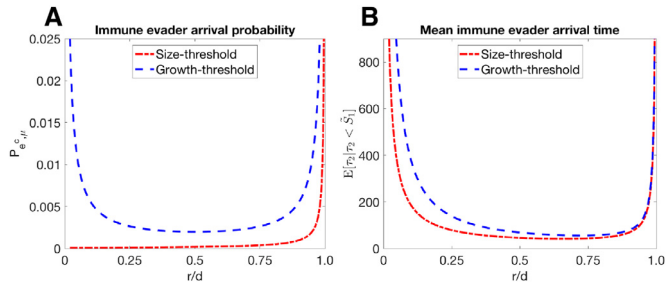

Fig. 3. Immune evader arrival probabiity and mean arrival time. (A) Immune evader arrival probability and (B) mean time of evader arrival for both growth-limited (blue, $R = 10^2$) and size-limited (red, $m_c = 10^3$) detection assumptions ($d = 0.2$, $\mu = 10^{-6}$).

3.2. Cancer sneak-through predicted by growth-limited detection exclusively

Non-escape E_e^c occurs with certainty under deterministic recognition. However, a dynamic threat may acquire an immune evader (event $E_{e^c,\mu}$). The probability of evader acquisition as a function of deterministic detection at size m is given by

$$P_{e^c,\mu}(m) = 1 - (1-\mu)^{m-1}\left(\frac{d-(1-\mu)r}{d-(1-2\mu)r}\right)^m. \tag{11}$$

This arrival probability is plotted in Fig. 3 alongside mean evader arrival times as a function of net growth rates r for size- and growth-limited detection assumptions (see SI for full details). Immune evaders rarely emerge for slow-growing threats under size-limited detection, and only do so on average over large time scales. This contrasts with growth-limited detection, for which immune evaders arrive with high probability for both large and small r, and do so with comparable time scales of arrival. Evasion behavior under the latter detection mode predicts for the first time a novel mechanism of sneak-through resulting exclusively from acquired immune evasion. A corollary to this implies that enhancements to the rate of immune killing (via increased d) alone cannot eliminate the risk of immune evader arrival, and the effects of such immunomodulation are diminished for slow-growth cancers. This prediction corroborates known experimental observations linking growth-rate with immune resiliency, including slow-growth melanoma variants with known T-cell exclusion (Spranger et al., 2015), and are reminiscent of the state of reduced proliferation with concomitant survival phenotypes characteristic of drug tolerant persisters (Chisholm et al., 2015), as well as the observed concave relationship between viral growth rate and peak CD8+ T-cell response (Bocharov et al., 2004) . We focus next on the case of a dynamic threat under adaptive immune recognition in subsequent sections.

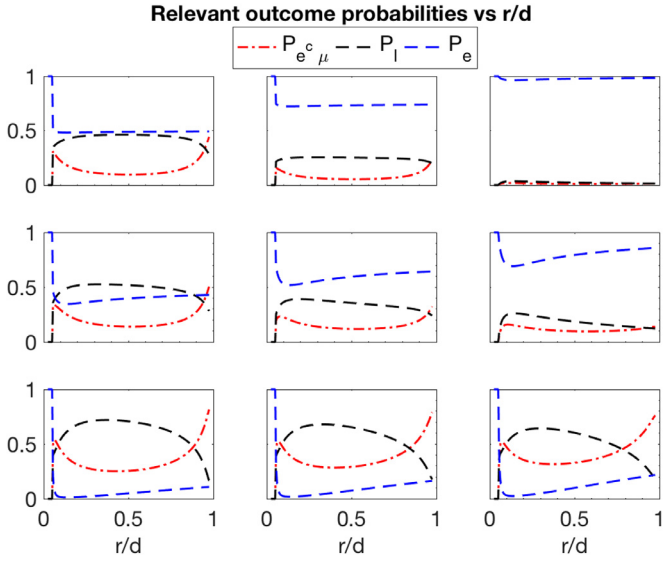

Fig. 4. Probability estimates of relevant immune outcomes. Dynamic threat escape, evasion, and loss probabilities as a function of relative net growth rate r/d for various values of immune turnover (rows bottom-to-top: $k = \{10^{-1}, 10^{-2}, 10^{-3}\}$) and repertoire diversity (columns left-to-right: $p_b = \{0.5, 0.75, 1.0\}$) ($d = 0.20$, $\mu = 10^{-6}$, $R = 10^4$, $M = 10^6$).

3.3. Acquired immune evasion and escape in the setting of compromised adaptive immunity

In contrast with the prior examples, a dynamic threat faced with an adaptive immune system has nontrivial likelihood of events E_e and E_μ. We focus here on escape E_e, immune evasion $E_{e^c,\mu}$, and cancer loss (immune victory) E_{e^c,μ^c} with respective probabilities P_e, $P_{e^c,\mu}$, and P_l. A similar analysis (Eq. S49) that marginalizes over the deterministic detection sizes in Eq. (11) is depicted for various immune parameters under growth-limited detection (Fig. 4). Under competent immune surveillance (high k, low p_b) disease stems almost exclusively from acquired immune evasion, and the majority of threats are expected to be cleared. However, as turnover rate and repertoire diversity are compromised, immune escape is predicted to dominate over acquired evasion in its overall contribution to cancer progression. Here, the overall predicted success probability of disease clearance, P_l, is again maximal for large and small r. In all cases, sneak-through is observed for slow growth threats, further supporting the growth-threshold conjecture under adaptive immune surveillance.

The dependence of disease mechanism on immune status predicts an essential role of immune recognition in the ability to control adaptive threats. Motivated by this, we apply our model to predict cancer incidence as a function of an aging immune compartment. We select AML as a representative case due to the large amount of available incidence data, its low mutation burden, association with advanced age, and, unlike solid malignancies, relative accessibility by the adaptive immune compartment (Alexandrov et al., 2013). Empirically observed decreases in thymic output in middle age and T-cell repertoire diversity in advanced age (Naylor et al., 2005) are modeled by decreasing Hill func-

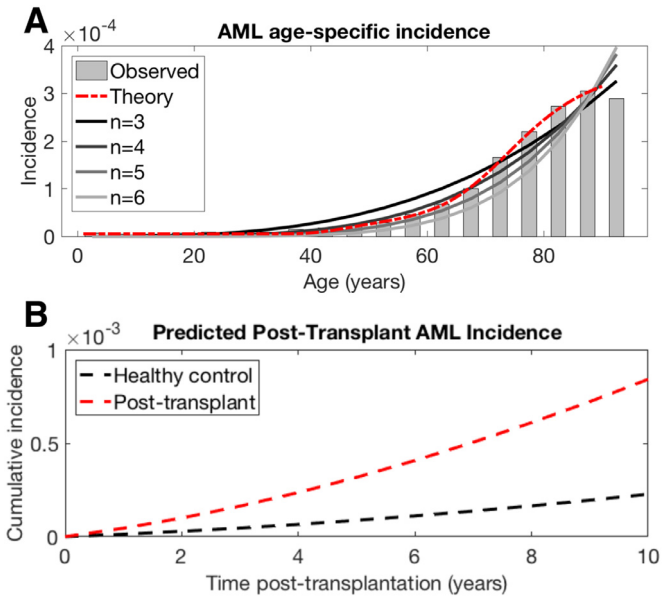

Fig. 5. AML incidence vs immune function. (A) Bar plot of empirical data (gray) is compared to model-derived AML estimate $P_e + P_{e^c,\mu}$ (red dashed line) that assumes constant cancer incidence and decreasing immunity vs age. Thymic turnover rates and effective clone sizes are modeled as Hill functions. Escape probability is approximated using $p_b \approx 1 - (1-\tilde{p})^{N_t}$, where $\tilde{p} \sim 10^{-6}$ is the probability of a single TCR recognizing the immune sensitive population and N_t is the effective number of distinct clones (See SI for details). This estimate is compared to the least squares best-fit models of multi-stage incidence (solid lines), where incidence is assumed to be approximately proportional to t^n, for age t and n number of hits.; (B) Predicted cumulative incidence over 10 years assuming chronic immunosuppression ($1 - p_b$ and k scaled by $\alpha = 0.9$) and mean age of 43 prior to treatment.

tions of k and $1-p_b$, respectively. While the absolute mapping between recognition probabilities via $p_r(m;\ m_0)$ and TCR diversity and turnover rates remains an open problem, we may use the known relative decreases in each of these parameters as a function of age in order to estimate potential immune impairment. The model assumes equal cancer risk for every age and estimates escape probability by incorporating the total number of T-cell clones, N_t, and the probability of a single T-cell recognizing individual antigenic peptide, $\tilde{p}$, via $p_b = (1-\tilde{p})^{N_t}$ as done previously (George et al., 2017). Incidence (defined as $1 - P_l$) for a particular set of parameters explains empirical AML data well, outperforming the standard multi-hit model of cancer incidence (Fig. 5A).

The model agreement with age-specific incidence data (Cancer Research UK, 2013) would suggest that age-incidence may be partitioned into three categories: Early, unfortunate disease due to the (rare) arrival of immune evaders that escape immune detection, slightly increased incidence in middle age secondary to lower turnover rates, and dramatic, late-onset increases in risk resulting from diminished TCR repertoire diversity. Our results are consistent with recent independent efforts to quantify immune-related cancer incidence (Palmer et al., 2018). The same parameter choice, assuming mild ($\sim$10%) decreases in T-cell recognition, is applied to characterize predicted AML incidence in the setting of chronic immunosuppression (Fig. 5B) and we find general agreement with large ($n \sim 3 \cdot 10^5$) empirical datasets of heart and lung transplant recipients and healthy controls (Offman et al., 2004).

4. Applications to immunotherapy

We now turn to the setting of adjuvant immunotherapy with the goal of estimating the therapeutic benefit of chimeric antigen receptor (CAR) T-cell and tumor antigen vaccination therapies. We introduce E to denote the event of overall disease elimination with corresponding probability equal to the sum of tumor loss probability due to immune system elimination (P_l above) and treatment probability, denoted by P_T. Treatment probability may be expanded by conditioning on relevant events:

$$P_T = \mathbb{P}\big(E \mid E_{e,\mu}\big)P_{e,\mu} + \mathbb{P}\big(E \mid E_{e,\mu^c}\big)P_{e,\mu^c} + \mathbb{P}\big(E \mid E_{e^c,\mu}\big)P_{e^c,\mu}. \qquad (12)$$

where the necessary conditioning probabilities are derived in the SI. We assume that radio- (or chemo-) ablative therapy administered at time of detection T_D and prior to adjuvant immunotherapy reduces the population to a minimal residual level $m_{mrd} \ll M$.

4.1. CAR T-cell therapy

Chimeric antigen receptor (CAR) T-cells are a class of *ex-vivo* engineered T-cells with artificial receptors and co-stimulatory signals designed to target an epitope differentially expressed by cancer cells (Sadelain et al., 2017). Their use has been particularly effective against hematological malignancies, wherein a variety of B-cell lymphomas demonstrate response to anti-CD-19 CAR T-cells (Brudno and Kochenderfer, 2018). Importantly, the CAR T-cell receptor is not limited to MHC-I recognition and can identify a variety of preferentially expressed tumor cell signatures, including surface proteins and carbohydrates (Yu et al., 2017). Thus, CAR T-cell therapy is effective in settings such as acute lymphoblastic leukemia, where mutation burden is low (Martin et al., 2016; Wang and Rivière, 2016). Its success in solid malignancies requires selection of preferentially over-expressed tumor-specific epitopes in the bulk tumor (Brown and Adusumilli, 2016; Newick et al., 2016).

Our analysis considers the case where a CAR T-cell clone has been engineered with recognition directed against a pre-identified tumor-specific epitope. We assume the CAR T-cell detection limit, m_{car}, is sufficiently low so that $m_{car} \le m_{mrd}$ (See SI for details). Deterministic detection therefore occurs immediately at size m_{mrd} for some fixed dosage of CAR T-cells as a result of built-in co-stimulation that occurs automatically with receptor binding. We allow for the arrival of CAR epitope-evasive cells at rate μ_{car} following treatment, and neglect the event that an epitope-evasive clone is present prior to treatment. Since CAR T-cells target all cancer cells at detection, successful treatment proceeds identically regardless of how the cancer population arrived at detection (escape vs evasion). Therefore, the conditional probabilities of Eq. (12) reduce to deterministic recognition with detection limit at starting size m_{mrd}, and may be written as a generalized version of Eq. (11).

Analytical estimates of CAR T-cell P_E are plotted over all growth ranges for a variety of immune states in Fig. 6 . $\mu_{car} \sim 10^{-4}$ was chosen large to best illustrate CAR T-cell efficacy vs growth rate. In reality, μ_{car} could be significantly less than μ depending on the CAR T-cell target, so that Fig. 6 underestimates CAR T-cell benefit. Intuitively, CAR T-cell therapy is predicted to impart substantial treatment benefit independent of immune functioning because CAR T-cell cancer elimination does not rely upon the host immune system. Detection at m_{mrd} is effectively size-limited, and so this therapy is also less effective against threats with larger net growth rates.

4.2. Autologous neoantigen vaccines

Autologous neoantigen vaccines are another type of immunotherapy which relies on the delivery of tumor antigens to the cell in order to augment or enhance the effect of neoantigen-specific CD8+ T-cells (Fritsch et al., 2014). Contrasting their reduced efficacy in tumors with lower mutation rates (Martin et al., 2016), neoantigen vaccines have been effective against highly mutagenic tumors, such as melanoma, where the neoantigen burden

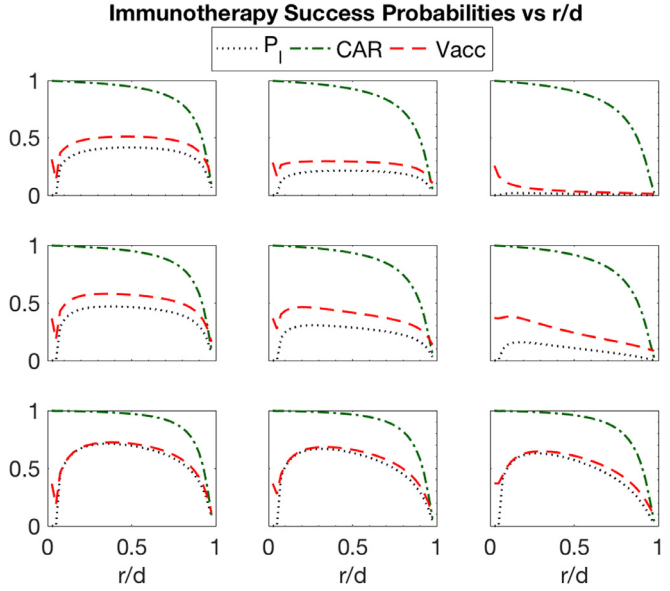

Fig. 6. Predicted disease elimination probability ($P_I + P_E$). CAR T-cell (green) and neoantigen vaccine (red) therapy benefits are compared to non-treatment survival predictions (black) as a function of relative net growth rate r/d for various values of immune turnover (rows bottom-to-top: $k = \{10^{-1}, 10^{-2}, 10^{-3}\}$) and repertoire diversity (columns left-to-right: $p_b = \{0.5,\ 0.75,\ 1.0\}$) ($d = 0.20$, $\mu = 10^{-6}$, $R = 10^4$, $M = 10^6$, $m_{mrd} = 10^3$, $R = 0$ for neoantigen vaccine case, $\mu_{car} = 10^{-4}$).

is significant (Hellmann and Snyder, 2017; Ott et al., 2017; Sahin et al., 2017). In our framework, successful immune priming occurs if sufficient levels of vaccine-delivered antigen suddenly become available for activating T-cells, effectively reducing the detection threshold R. For simplicity we assume that a sufficient level of tumor antigens are present so that $R = 0$ and any residual cancer size can be targeted.

Unlike CAR T-cell treatment, vaccine therapy is only successful when there is an absence of immune evasive cells both prior to and following treatment (i.e. on E_{μ^c}), since type-2 cells can still evade vaccine-sensitized host T-cells. The only conditional probability in Eq. (12) that contributes to treatment success is $\mathbb{P}\left(E|E_{e,\mu^c}\right)$, which is none other than P_I in the adaptive model with detection and initial population size both equal to m_{mrd} (see SI). The final required quantity is the factor P_{e,μ^c} calculated as follows:

$$P_{e,\mu^c} = \mathbb{P}\left(E_{\mu^c} \mid E_e\right) P_e = (1-\mu)^M \cdot P_e\left(M; m_0\right). \tag{13}$$

Vaccine treatment efficacy is plotted alongside CAR T-cell therapy in Fig. 6. There is minimal predicted treatment benefit in immunocompromized patients, consistent with the fact that vaccine strategies are reliant upon proper immune recognition. The treatment benefit appears to be maximal for patients with preserved repertoire diversity and low T-cell turnover, presumably the result of allowing more time to pass, and hence immune turnover to occur, at low population sizes. Elimination of slow-growth threats that would normally progress via sneak-through is increased, since there is no post-treatment detection limit.

5. Discussion

Our findings support the importance of the growth-threshold conjecture as an essential aspect of empirical recognition dynamics, since size-limited detection predicts an exclusive preference for fast-growing threats. In addition to static growth and recognition, sneak-through is predicted by a new mechanism that involves preferential acquisition of immune evasion for slow and large growth rates.

Application of this relatively simple model to AML provides a quantification of the trade-off between T-cell turnover and repertoire size and control of malignancy. Moreover,the assumption that incidence carries equal risk through time places no mechanistic restrictions on the molecular generation of tumor development, and stands as a prediction of tumor generation largely orthogonal to the canonical multi-hit hypothesis (Armitage and Doll, 1954). We find not only that this model agrees more closely with the data when compared to the best-fit multi-hit predictions, but that the immune incidence curve also accurately reproduces the sigmoid shape of AML incidence in a way that is impossible for the convex multi-hit model. It is also interesting that gender-specific differences in thymic output (favoring females) also correlate with a systematic reduction in AML incidence (Pido-Lopez et al., 2001). From a clinical standpoint, the prediction of maximizing immune health in order to mitigate incidence is broadly quantified for tumors that may adopt immune evasion strategies, as well as more general immune threats. In the case of treatment-refractory AML with subsequent hematopoietic stem cell transplant, our results would suggest that particular emphasis should be placed on maintaining repertoire diversity and, where possible, thymic turnover (Holländer et al., 2010).

In an attempt to provide an initial and straightforward presentation, we assumed pure birth in the recognition and death phase. Future analysis using the more complicated birth-death process would likely increase the rate of immune evasion generation during immune killing. We have also assumed that immune killing occurs quickly and to a sufficient level for all threat sizes and that the threat net growth rate is fixed. We believe that this is a reasonable assumption for studying a rapidly growing threat such as AML, where reduced growth occurs only in advanced disease (Akinduro et al., 2018). Other dynamic threats including many solid tumors, which are characterized by complicated, time-varying growth rates, are analytically intractable in this framework and necessitate a more extensive reliance on numerical simulation. In general, for sigmoid growth, the above results assuming mean exponential growth provide an upper-estimate on tumor escape, while evasion under growth-limited detection inherently depends on the functional form of the growth rate. Though an approximation, we believe these dynamics are reasonable as a naïve T-cell clone expands rapidly, though not instantaneously, to become a dominant clone during proper immune activation (Desponds et al., 2016).

We selected AML as a model disease for initial assessment of our model owing to several applicable features. Its rapid growth is well-approximated by a growth rate homogeneous in time and size. Unlike their solid counterparts, the immune cells have no difficulty interfacing with hematological cancer cells. Lastly, AML's characteristically low mutational burden enables us to estimate immune evasion in the simplified framework above without the risk of ignoring possibly many intermediate phenotypes with mild evasion potential. It is likely however that the tumor-immune coevolution described here applies broadly to many cancer types, and therefore warrants careful consideration of other relevant factors, such as mutational burden and immune infiltration, in future analyses (Blank et al., 2016).

The advantage of antigen vaccine strategies studied here resulted from augmented immune priming of the T-cell repertoire, thereby allowing recognition to overcome detection limits. Variations due to cancer subtype, including antigenicity and (for solid tumors) T-cell infiltration, may substantially affect immune priming, and hence vaccine efficacy, but are not considered here. In particular, the subclonal neoantigen landscape is an important consideration that warrants further analysis for a more complete under-

standing. Future studies will further distinguish between clones of differing fitnesses dependent upon their antigenicity and intermediate levels of immune evasion in an attempt to better characterize the co-evolution between a dynamic tumor and adaptive immune compartment.

Author's contribution

J.T.G. conceived of and designed the research, analyzed the data, contributed new analytic equations, and wrote the manuscript. H.L. designed research, analyzed the data, contributed new analytic equations, and wrote the manuscript.

Both authors have approved the final article.

Acknowledgments

We would like to thank Rainer Lanz for valuable feedback on the manuscript draft and Jeffrey Molldrem for fruitful discussions on AML immunotherapy. J.T.G. is supported by the National Cancer Institute of the National Institutes of Health (F30CA213878). H.L. is supported by Cancer Prevention and Research Institute of Texas Scholars program (R1111).

Supplementary material

Supplementary material associated with this article can be found, in the online version, at doi:10.1016/j.jtbi.2018.09.012.

References

Akinduro, O., Weber, T., Ang, H., Haltalli, M., Ruivo, N., Duarte, D., Rashidi, N., Hawkins, E., Duffy, K., Celso, C.L., 2018. Proliferation dynamics of acute myeloid leukaemia and haematopoietic progenitors competing for bone marrow space. Nat. Commun. 9 (1), 519.

Alexandrov, L.B., Nik-Zainal, S., Wedge, D.C., Aparicio, S.A., Behjati, S., Biankin, A.V., Bignell, G.R., Bolli, N., Borg, A., Børresen-Dale, A.-L., et al., 2013. Signatures of mutational processes in human cancer. Nature 500 (7463), 415.

Alsaab, H.O., Sau, S., Alzhrani, R., Tatiparti, K., Bhise, K., Kashaw, S.K., Iyer, A.K., 2017. Pd-1 and pd-l1 checkpoint signaling inhibition for cancer immunotherapy: mechanism, combinations, and clinical outcome. Front. Pharmacol. 8, 561.

Andrew, S.M., Baker, C.T.H., Bocharov, G.A., 2007. Rival approaches to mathematical modelling in immunology. J. Comput. Appl. Math. 205 (2), 669–686. doi:10.1016/j.cam.2006.03.035.

Arias, C.F., Herrero, M.A., Cuesta, J.A., Acosta, F.J., Fernandez-Arias, C., 2015. The growth threshold conjecture: a theoretical framework for understanding T-cell tolerance. R. Soc. Open Sci. 2 (7), 150016. doi:10.1098/rsos.150016.

Armitage, P., Doll, R., 1954. The age distribution of cancer and a multi-stage theory of carcinogenesis. Br. J. Cancer 8 (1), 1.

Blank, C.U., Haanen, J.B., Ribas, A., Schumacher, T.N., 2016. The cancer immunogram. Science 352 (6286), 658–660.

Bocharov, G., Ludewig, B., Bertoletti, A., Klenerman, P., Junt, T., Krebs, P., Fraser, C., Anderson, R.M., Luzyanina, T., 2004. Underwhelming the immune response : effect of slow virus growth on CD8+ T-Lymphocyte responses. J. Virol. 78 (5), 2247–2254. doi:10.1128/JVI.78.5.2247.

Bronte, V., Mocellin, S., 2009. Suppressive influences in the immune response to cancer. J. Immunother. 32 (1), 1–11.

Brown, C.E., Adusumilli, P.S., 2016. Next frontiers in CAR T-cell therapy. Mol. Ther. Oncolytics 3, 16028. doi:10.1038/mto.2016.28.

Brudno, J.N., Kochenderfer, J.N., 2018. Chimeric antigen receptor T-cell therapies for lymphoma. Nat. Rev. Clin. Oncol. 15 (1), 31.

del Campo, A.B., Kyte, J.A., Carretero, J., Zinchencko, S., Méndez, R., González-Aseguinolaza, G., Ruiz-Cabello, F., Aamdal, S., Gaudernack, G., Garrido, F., et al., 2014. Immune escape of cancer cells with beta2-microglobulin loss over the course of metastatic melanoma. Int. J. Cancer 134 (1), 102–113.

Cancer Research UK, 2013. Acute myeloid leukaemia (AML) incidence by age. http://www.cancerresearchuk.org/health-professional/cancer-statistics/statistics-by-cancer-type/leukaemia-aml/incidence (accessed 2017-09-01).

Carretero, R., Romero, J.M., Ruiz-Cabello, F., Maleno, I., Rodriguez, F., Camacho, F.M., Real, L.M., Garrido, F., Cabrera, T., 2008. Analysis of HLA class I expression in progressing and regressing metastatic melanoma lesions after immunotherapy. Immunogenetics 60 (8), 439.

Chisholm, R.H., Lorenzi, T., Lorz, A., Larsen, A.K., Almeida, L., Escargueil, A., Clairambault, J., 2015. Emergence of drug tolerance in cancer cell populations: an evolutionary outcome of selection, non-genetic instability and stress-induced adaptation. Cancer Res. canres–2103.

Couzin-Frankel, J., 2013. Cancer immunotherapy. Science 342 (6165), 1432–1433.

Desponds, J., Mora, T., Walczak, A.M., 2016. Fluctuating fitness shapes the clone-size distribution of immune repertoires. Proc. Natl. Acad. Sci. 113 (2), 274–279.

Driessens, G., Kline, J., Gajewski, T.F., 2009. Costimulatory and coinhibitory receptors in anti-tumor immunity. Immunol. Rev. 229 (1), 126–144.

Dunn, G.P., Bruce, A.T., Ikeda, H., Old, L.J., Schreiber, R.D., 2002. Cancer immunoediting: from immunosurveillance to tumor escape. Nat. Immunol. 3 (11), 991–998. doi:10.1038/ni1102-991.

Fridman, W.H., Mlecnik, B., Bindea, G., Pagès, F., Galon, J., 2011. Immunosurveillance in human non-viral cancers. Curr. Opin. Immunol. 23 (2), 272–278. doi:10.1016/j.coi.2010.12.011.

Fritsch, E.F., Hacohen, N., Wu, C.J., 2014. Personal neoantigen cancer vaccines: the momentum builds. Oncoimmunology 3 (6), e29311. doi:10.4161/onci.29311.

Garrido, F., Aptsiauri, N., Doorduijn, E.M., Lora, A.M.G., van Hall, T., 2016. The urgent need to recover MHC class I in cancers for effective immunotherapy. Curr. Opin. Immunol. 39, 44–51.

George, J.T., Kessler, D.A., Levine, H., 2017. Effects of thymic selection on T cell recognition of foreign and tumor antigenic peptides. Proc. Natl. Acad. Sci. 201708573.

George, J.T., Levine, H., 2018. Stochastic trajectories and escape probabilities for immune evasion of a static threat. Data Brief Submitted.

Grossman, Z., Paul, W.E., 1992. Adaptive cellular interactions in the immune system: the tunable activation threshold and the significance of subthreshold responses. Proc. Natl. Acad. Sci. 89 (21), 10365–10369. doi:10.1073/pnas.89.21.10365.

Hellmann, M. D., Snyder, A., 2017. Making it personal: neoantigen vaccines in metastatic melanoma. doi:10.1016/j.immuni.2017.08.001.

Herbst, R.S., Soria, J.-C., Kowanetz, M., Fine, G.D., Hamid, O., Gordon, M.S., Sosman, J.A., McDermott, D.F., Powderly, J.D., Gettinger, S.N., et al., 2014. Predictive correlates of response to the anti-pd-l1 antibody mpdl3280a in cancer patients. Nature 515 (7528), 563.

Holländer, G.A., Krenger, W., Blazar, B.R., 2010. Emerging strategies to boost thymic function. Curr. Opin. Pharmacol. 10 (4), 443–453.

Iwasa, Y., Nowak, M.A., Michor, F., 2006. Evolution of resistance during clonal expansion. Genetics 172 (4), 2557–2566.

Johansen, P., Storni, T., Rettig, L., Qiu, Z., Der-Sarkissian, A., Smith, K.A., Manolova, V., Lang, K.S., Senti, G., Mullhaupt, B., Gerlach, T., Speck, R.F., Bot, A., Kundig, T.M., 2008. Antigen kinetics determines immune reactivity. Proc. Natl. Acad. Sci. 105 (13), 5189–5194. doi:10.1073/pnas.0706296105.

Khailaie, S., Bahrami, F., Janahmadi, M., Milanez-Almeida, P., Huehn, J., Meyer-Hermann, M., 2013. A mathematical model of immune activation with a unified self-nonself concept. Front. Immunol. 4 (474), 1–19. doi:10.3389/fimmu.2013.00474.

Kirschner, D., Panetta, J.C., 1998. Modeling immunotherapy of the tumor - immune interaction. J. Math. Biol. 37 (3), 235–252. doi:10.1007/s002850050127.

Leach, D.R., Krummel, M.F., Allison, J.P., et al., 1996. Enhancement of antitumor immunity by CTLA-4 blockade. Science 271 (5256), 1734–1736.

Lin, A., Yan, W.-H., 2015. Human leukocyte antigen-g (HLA-G) expression in cancers: roles in immune evasion, metastasis and target for therapy. Mol. Med. 21 (1), 782.

Martin, S.D., Brown, S.D., Wick, D.A., Nielsen, J.S., Kroeger, D.R., Twumasi-Boateng, K., Holt, R.A., Nelson, B.H., 2016. Low mutation burden in ovarian cancer may limit the utility of neoantigen-targeted vaccines. PLoS One 11 (5), e0155189. doi:10.1371/journal.pone.0155189.

Michor, F., Iwasa, Y., Nowak, M.A., 2004. Dynamics of cancer progression. Nat. Rev. Cancer 4 (3), 197–205.

Nani, F.K., OÇŞuztöreli, M.N., 1994. Modelling and simulation of Rosenberg-type adoptive cellular immunotherapy. Math. Med. Biol. 11 (2), 107–147. doi:10.1093/imammb/11.2.107.

Naylor, K., Li, G., Vallejo, A.N., Lee, W.-W., Koetz, K., Bryl, E., Witkowski, J., Fulbright, J., Weyand, C.M., Goronzy, J.J., 2005. The influence of age on T cell generation and TCR diversity. J. Immunol. 174 (11), 7446–7452.

Newick, K., Moon, E., Albelda, S.M., 2016. Chimeric antigen receptor T-cell therapy for solid tumors. Mol. Ther. Oncolytics 3 (October 2015), 16006. doi:10.1038/mto.2016.6.

Offman, J., Opelz, G., Doehler, B., Cummins, D., Halil, O., Banner, N.R., Burke, M.M., Sullivan, D., Macpherson, P., Karran, P., 2004. Defective DNA mismatch repair in acute myeloid leukemia/myelodysplastic syndrome after organ transplantation. Blood 104 (3), 822–828.

Ott, P.A., Hu, Z., Keskin, D.B., Shukla, S.A., Sun, J., Bozym, D.J., Zhang, W., Luoma, A., Giobbie-Hurder, A., Peter, L., Chen, C., Olive, O., Carter, T.A., Li, S., Lieb, D.J., Eisenhaure, T., Gjini, E., Stevens, J., Lane, W.J., Javeri, I., Nellaiappan, K., Salazar, A.M., Daley, H., Seaman, M., Buchbinder, E.I., Yoon, C.H., Harden, M., Lennon, N., Gabriel, S., Rodig, S.J., Barouch, D.H., Aster, J.C., Getz, G., Wucherpfennig, K., Neuberg, D., Ritz, J., Lander, E.S., Fritsch, E.F., Hacohen, N., Wu, C.J., 2017. An immunogenic personal neoantigen vaccine for patients with melanoma. Nature 547, 217–221. doi:10.1038/nature22991.

Palmer, S., Albergante, L., Blackburn, C.C., Newman, T., 2018. Thymic involution and rising disease incidence with age. Proc. Natl. Acad. Sci. 115 (8), 1883–1888.

Pido-Lopez, J., Imami, N., Aspinall, R., 2001. Both age and gender affect thymic output: more recent thymic migrants in females than males as they age. Clin. Exp. Immunol. 409–413.

Pradeu, T., Jaeger, S., Vivier, E., 2013. The speed of change: towards a discontinuity theory of immunity? Nat. Rev. Immunol. 13 (10), 764–769. doi:10.1038/nri3521.

Sadelain, M., Rivière, I., Riddell, S., 2017. Therapeutic T cell engineering. Nature 545 (7655), 423–431. doi:10.1038/nature22395.

Sahin, U., Derhovanessian, E., Miller, M., Kloke, B.-p., Simon, P., Löwer, M., Bukur, V., Tadmor, A.D., Luxemburger, U., Schrörs, B., Omokoko, T., Vormehr, M., Albrecht, C., Paruzynski, A., Kuhn, A.N., Buck, J., Heesch, S., Schreeb, K.H., Müller, F., Ortseifer, I., Vogler, I., Godehardt, E., Attig, S., Rae, R., Breitkreuz, A., Tolliver, C., Suchan, M., Martic, G., Hohberger, A., Sorn, P., Diekmann, J., Ciesla, J.,

Waksmann, O., Brück, A.-k., Witt, M., Zillgen, M., Rothermel, A., Kasemann, B., Langer, D., Bolte, S., Diken, M., Kreiter, S., Nemecek, R., Gebhardt, C., Grabbe, S., Höller, C., Utikal, J., Huber, C., Loquai, C., Türeci, Ö., 2017. Personalized RNA mutanome vaccines mobilize poly-specific therapeutic immunity against cancer. Nature 547 (7662), 222–226. doi:10.1038/nature23003.

Sheu, J., Shih, I.-M., 2010. HLA-G and immune evasion in cancer cells. J. Formos. Med. Assoc. 109 (4), 248–257.

Sontag, E.D., 2017. A dynamic model of immune responses to antigen presentation predicts different regions of tumor or pathogen elimination. Cell Syst. 4, 231–241.

Spranger, S., Bao, R., Gajewski, T.F., 2015. Melanoma-intrinsic β-catenin signalling prevents anti-tumour immunity. Nature 523 (7559), 231.

Straten, T.P., Garrido, F., 2016. Targetless T cells in cancer immunotherapy. J. Immunother. Cancer 4 (1), 23.

Tripathi, S.C., Peters, H.L., Taguchi, A., Katayama, H., Wang, H., Momin, A., Jolly, M.K., Celiktas, M., Rodriguez-Canales, J., Liu, H., et al., 2016. Immunoproteasome deficiency is a feature of non-small cell lung cancer with a mesenchymal phenotype and is associated with a poor outcome. Proc. Natl. Acad. Sci. 113 (11), E1555–E1564.

Wang, X., Rivière, I., 2016. Clinical manufacturing of CAR T cells: foundation of a promising therapy. Mol. Ther. Oncolytics 3 (February), 1–7. doi:10.1038/mto.2016.15.

Yu, S., Li, A., Liu, Q., Li, T., Yuan, X., Han, X., Wu, K., 2017. Chimeric antigen receptor T cells: a novel therapy for solid tumors. J. Hematol. Oncol. 10 (1), 78.

Supplementary Information: Stochastic modeling of tumor progression and immune evasion

Jason T. George and Herbert Levine

September 18, 2018

S1 Overview

Here, we provide additional details and analysis of the models considered in the main text; growth-limited vs. size-limited detection modes, deterministic vs. stochastic (adaptive) recognition, and static vs. dynamic (immune evading) threats. We begin in Section S2 by describing minimal detection sizes as well as mean detection and elimination times. In Section S3 we specify the recognition and evasion probabilities for an adaptive threat. Section S4 details the general results for static threat escape probabilities and optimal growth strategies for static threats under growth-limited vs. size-limited detection as well as deterministic vs. stochastic recognition. This analysis is repeated for dynamical threats in Section S5, adding estimates of immune evasion probabilities and mean evasion arrival times. In section S6 we elaborate on the constitutive assumptions used to characterize turnover rate and immune repertoire diversity as functions of time in the calculation of age-dependent AML incidence, and Section S7 concludes with a quantitative framework for predicting successful immunotherapy treatment.

S2 Mean detection and elimination times

We assume throughout that population dynamics follow transition equations given by Eqs. 1-2 in the main text. Let $X_1(t)$ denote the population size of sensitive invading cells, r the per-cell net growth rate, $M \gg 1$ the terminal size, m the size at which the population is recognized, and m_0 the minimal population size at which immune recognition may first occur. Under the growth-threshold conjecture, immune recognition may only begin once $rX_1(t) \geq R$, for a lower limit of detection R of the total invading threat net growth rate. Thus,

$$m_0(r) = \lceil R/r \rceil. \tag{S1}$$

In order to avoid confusion, we will denote the detection size in the size-limited case as

$$m_0 = m_c. \tag{S2}$$

In the deterministic case, recognition occurs with certainty once $X_1 = m = m_0$. In the stochastic case, recognition and subsequent killing may (or may not) occur at any size $X_1 = m$ for $m_0 \leq m \leq M$.

Let S_1 be the time at which X_1 becomes recognized, and $\tilde{S}_1$ the time at which X_1 reaches extinction conditioned on initial recognition at size m. Let T_i be the time that the population grows to size i during the growth phase, and $\tilde{T}_i$ the time that the population dies to size i during the death phase, with corresponding mean times t_i and $\tilde{t}_i$, respectively. Then $X_1(t) = i$ on time intervals $[T_i, T_{i+1})$, and $[\tilde{T}_i, \tilde{T}_{i-1})$ with $T_1 = 0$ and $\tilde{T}_m = T_m$. Similarly, let $\Delta T_i = T_{i+1} - T_i$ (resp. $\Delta \tilde{T}_i = \tilde{T}_{i-1} - \tilde{T}_i$) denote the exponentially-distributed inter-arrival time at population size $X_1 = i$ during growth (resp. immune killing) with mean time Δt_i (resp. $\Delta \tilde{t}_i$). Then, for $h_i \equiv \sum_{j=1}^{i} 1/j$ and $m \gg 1$, we have that $t_i = h_{i-1}/r$, and the mean detection and elimination times are given by

$$\mathbb{E}[S_1] = \sum_{i=1}^{m-1} \mathbb{E}[\Delta T_i] = \sum_{i=1}^{m-1} \Delta t_i = \frac{h_{m-1}}{r} \approx \frac{\log m}{r}, \tag{S3}$$

and

$$\mathbb{E}[\tilde{S}_1] = \mathbb{E}[S_1] + \sum_{i=1}^{m} \Delta \tilde{t}_i = \frac{h_{m-1}}{r} + \frac{h_m}{\tilde{r}} \approx \frac{d \log m}{r(d-r)}. \tag{S4}$$

Where appropriate, mean inter-arrival times will be used as approximations to simplify calculations. The effects of varying net growth rate on mean population dynamics are given in Fig. S1. Small differences in growth rates for rapidly growing threats primarily affect the time spent in the death phase and result in minimal differences in detection sizes. This is in contrast to slow-growth threats, which all become quickly eliminated by a robust immune response, but are recognized at a variety of different sizes. In the extreme cases (not pictured), threats outgrow the immune system death rate, or grow so slowly that they escape detection altogether.

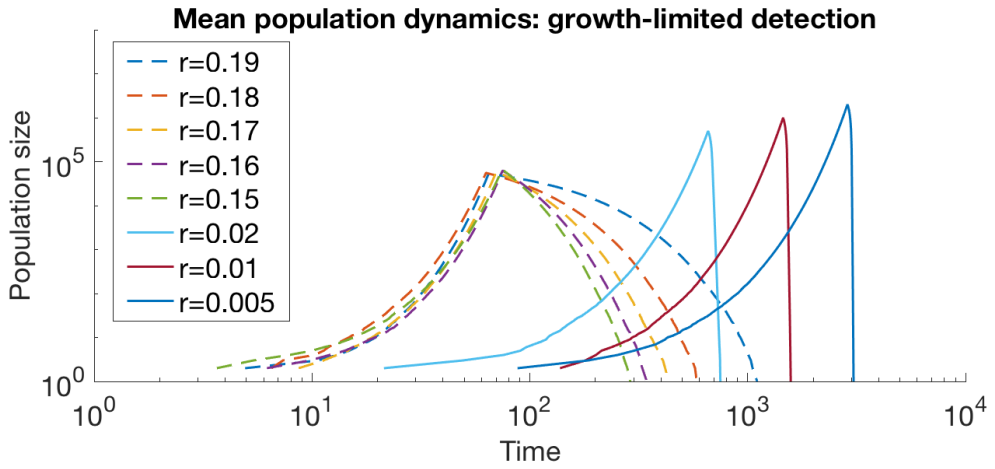

Figure S1: Population dynamics for a static threat under growth-limited, deterministic detection. Mean population dynamics for various large (dashed) and small (solid) net growth rates r ($d = 0.20, R = 10^4, M = 10^7$, each trajectory averaged $n = 10$ times).

S3 Immune recognition

We model immune recognition of a growing threat with two parameters. The first parameter represents a measure of immune repertoire diversity in the form of a background escape probability, p_b, so that immunocompetent systems with high repertoire diversity have low escape probabilities. p_b characterizes the likelihood of response from a fixed immune repertoire or innate immune system when the threat first becomes detectable. Therefore, X_1 is recognized by the immune system at size m_0 with probability $1 - p_b$. The second parameter k represents the turnover rate of the adaptive immune compartment so that under adaptive recognition, threats may escape at size m_0, but eventually become detected for some size $m > m_0$.

S3.1 Deterministic recognition

Under deterministic recognition, $k = 0$ and $p_b = 0$ so that threats are recognized at size $m = m_0$. This provides a convenient starting point for the slightly more general setting of adaptive recognition.

S3.2 Adaptive recognition

In this case, the escape probability $p_b > 0$ represents the likelihood that a threat escapes the current immune repertoire immediately following the population's arrival to detectable size. Recognition therefore occurs at this moment with probability $1 - p_b$ and, should this occur, we have that $m = m_0$. Immune recognition due to turnover of the adaptive T-cell repertoire may also occur for $m_0 \leq m \leq M$. Adaptive recognition is modeled by the random arrival of recognizing T-cells at Poisson rate $k(t)$ for $X_1 \in \{m_0, \ldots, M\}$. The probability $P_a(m; m_0)$ that a threat escapes adaptive immune turnover to size m from initial detection size m_0 is given by

$$P_a(m; m_0) = \exp\left(- \int_{T_{m_0}}^{T_m} k(\tau) d\tau \right). \tag{S5}$$

For homogeneous T-cell turnover over time interval $\Delta T \equiv T_m - T_{m_0}$, this simplifies to

$$P_a(m; m_0) = e^{-k\Delta T}. \tag{S6}$$

The mean acquired escape probability can be calculated by noting that the inter-arrival times ΔT_j are independent exponential random variables as follows:

$$p_a(m;m_0) \equiv \mathbb{E}[P_a(m;m_0)] = \mathbb{E}\Big[\exp\Big\{-k\sum_{i=m_0}^{m-1}\Delta T_i\Big\}\Big] = \prod_{j=m_0}^{m-1}\mathbb{E}\big[e^{-k\Delta T_i}\big] = \prod_{j=m_0}^{m}\mathbb{E}\big[e^{-Y_i}\big] \tag{S7}$$

for $m > m_0$ and $Y_i \sim \text{Exp}(ri/k)$. The Moment-generating function, $M_{Y_i}(t)$, of Y_i is given by

$$M_{Y_i}(t) \equiv \mathbb{E}\big[e^{tY_i}\big] = \frac{1}{1-(kt/ri)}, \quad \text{for } t < ri/k. \tag{S8}$$

It follows by evaluating each M_{Y_i} at $t=-1$ that

$$p_a(m;m_0) = \prod_{i=m_0}^{m}\frac{ri}{ri+k}. \tag{S9}$$

When convenient, we apply the deterministic approximation by use of $\Delta t \equiv \mathbb{E}[\Delta T]$ as a lower-bound on the escape probability through Jensen's inequality:

$$p_a(m;m_0) \geq e^{-k\Delta t} \approx \left(\frac{m_0-1}{m-1}\right)^{k/r} \approx \big(m_0/m\big)^{k/r}. \tag{S10}$$

This estimate is sufficiently accurate under reasonable modeling assumptions with maximum error given by

$$||p_a(m,r) - e^{-k\Delta t}||_\infty < 0.017 \tag{S11}$$

over a parameter range that covers all of the values used in the analysis to follow (m ranging from 10^2 to 10^7 for all combinations of $m_0 = \{10^2, 10^3, 10^4\}$ and $k = \{10^{-1}, 10^{-2}, 10^{-3}\}$). We proceed by using this estimate to characterize p_a subsequently and throughout the main text. From this, we may approximate the total probability $p_e(m;m_0)$ that a threat escapes recognition from $X_1(t_{m_0}) = m_0$ to $X_1(t_m) = m$ by

$$p_e(m;m_0) = \begin{cases} 1, & m < m_0; \\ p_b\big(\frac{m_0}{m}\big)^{k/r}, & m_0 \leq m \leq M. \end{cases} \tag{S12}$$

We may also express via Eqs. S3-S12 the probability $p_r(m;m_0)$ that immune recognition first occurs while $X_1 = m$. Note that if $m = m_0$, then

$$p_r(m_0;m_0) = \big(1-p_b\big) + p_b\big[1-p_a(m_0+1;m_0)\big], \tag{S13}$$

and for $m > m_0$

$$p_r(m;m_0) = p_b p_a(m;m_0)\big[1-p_a(m+1;m)\big]. \tag{S14}$$

Together, we approximate p_r by

$$p_r(m;m_0) = \begin{cases} 0, & m < m_0; \\ 1-p_b e^{-\frac{k}{rm_0}}, & m = m_0; \\ p_b\Big(1-e^{-\frac{k}{rm}}\Big)\Big(\frac{m_0}{m}\Big)^{k/r}, & m_0 < m \leq M. \end{cases} \tag{S15}$$

Of course, $p_e = 1$ and $p_r = 0$ if $m_0 \geq M$, which only occurs trivially under size-limited detection if $m_c < M$ but may occur during growth-limited detection for r sufficiently small. The cumulative recognition probability $1 - p_e$ along with p_e and p_r will be applied to the subsequent sections on adaptive immune response.

S4 Static threats

In this section, an initial population of cells may undergo net growth to detection but do so without acquiring an immune evasive subpopulation. We wish to describe conditions under which non-evasive (static) immune threats may succeed in immune system evasion. In this case, a threat either escapes to detection size, denoted by event E_e with corresponding probability P_e, or is recognized and eliminated (denoted by E_e^c) , so that

$$\mathbb{P}(E_e) = P_e; \qquad \mathbb{P}(E_e^c) = 1 - P_e. \tag{S16}$$

S4.1 Growth strategies for static threats

Here we discuss growth strategies that result in static threat escape for growth-limited vs. size-limited detection assumptions under deterministic recognition followed by a similar analysis for adaptive recognition.

S4.1.1 Deterministic recognition

Deterministic recognition is a special case of Eq. S15 with $p_b = 0$, giving recognition probability unit mass at detection threshold so that

$$p_r(m; m_0) = \begin{cases} 0, & m \neq m_0; \\ 1, & m = m_0. \end{cases} \tag{S17}$$

Size-limited detection: If the immune system mounts a predictable response at size $m_0 \leq M$, then there is no preferred growth strategy under the size-threshold assumption aside from the case when $r > d$, since every threat is identified and eliminated at fixed size $m_c \leq M$. In this case,

$$P_e = \begin{cases} 1, & r > d; \\ 0, & r \leq d. \end{cases} \tag{S18}$$

Growth-limited detection: Under the growth-threshold assumption, slow-growth threats may 'sneak through' if $r < R/M$. Threats growing faster than R/M but not exceeding the immune killing rate are eliminated. In this case,

$$P_e = \begin{cases} 1, & r > d; \\ 0, & R/M < r \leq d; \\ 1, & r \leq R/M. \end{cases} \tag{S19}$$

The per-cell killing rate of a robust immune response is assumed to be much larger than the growth rate of most threats, and so when studying a population of dividing cancer cells, we generally restrict our attention to cases when $r < d$.

S4.1.2 Adaptive immune recognition

Evasion of the adaptive immune system occurs if the growing threat remains undetected for all sizes $m \in \{m_0, \ldots, M\}$. This in turn is related to the mean sojourn time of X_1 in $[m_0, M]$, given by

$$\Delta t_s(r) \approx \log\big(M/m_0\big) r^{-1}. \tag{S20}$$

By Eqs. S10, S12 we have that maximizing escape probability amounts to minimizing Eq. S20.

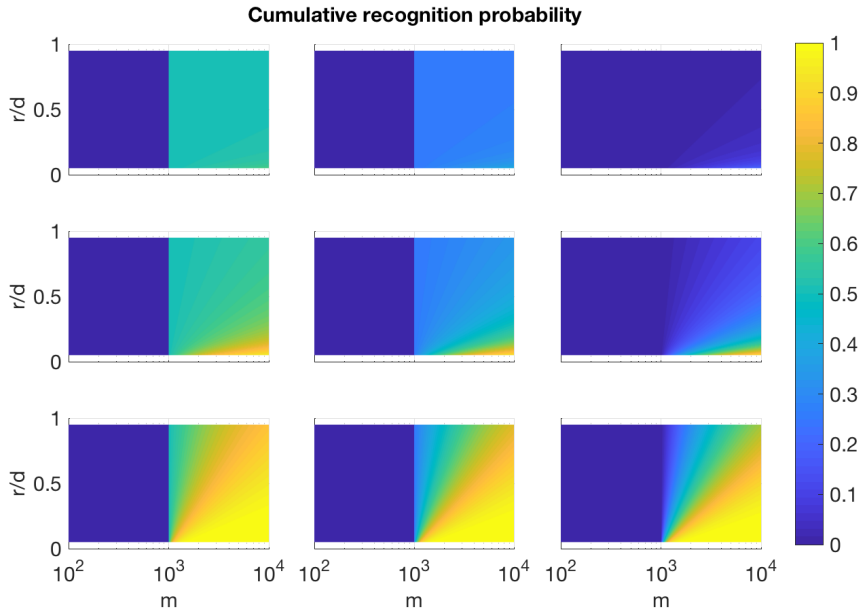

Figure S2: Cumulative recognition probabilities under adaptive, size-limited detection. The cumulative recognition probability, $1 - p_e(m; m_c)$, is given as a function of current population size (x-axis m) and net growth rate (y-axis r). This relation is plotted for varied escape probabilities across columns (left-to-right) $p_b = \{0.5, 0.75, 1.0\}$ and repertoire turnover rates across rows (bottom-to-top) $k \in \{10^{-1}, 10^{-2}, 10^{-3}\}$. In all cases, detection size $m_c = 10^3$, and faster growing threats have lower chances of detection than their slower growing counterparts.

Size-limited detection: Under the size-threshold assumption Eq. S20 becomes

$$\Delta t_s(r) \approx \log\big(M/m_c\big) r^{-1}, \tag{S21}$$

a decreasing function on $r \in (0, \infty)$. This therefore suggests that evasive populations which evolve over time to maximize their net growth rate have the best chance of avoiding elimination. The escape probability may be approximated via Eq. S12 with $m_0 = m_c$ and $m = M$, given by

$$P_e = p_b \Big(\frac{m_c}{M}\Big)^{k/r}. \tag{S22}$$

Growth-limited detection: Under the growth-threshold assumption, Eq. S20 becomes

$$\Delta t_s(r) \approx \log\left(\frac{rM}{R}\right) r^{-1}. \tag{S23}$$

Eq. S23 is continuous in r, increasing on $\big[R/M, eR/M\big)$ and decreasing on $\big(eR/M, \infty\big)$ with $\Delta t_s\big(R/M\big) = 0$. This supports the existence of a slow-growth window $r \in \big(R/M, eR/M\big)$ on which immune threats locally prefer decreased growth rates to obtain larger escape probabilities until an extreme value $r = R/M$ is achieved. Immune threats are predicted to grow free of immune detection below this threshold. The escape probability is given via Eq. S12 with $m_0 = \lceil R/r \rceil$. The cumulative recognition probability $1 - p_e(m; m_0)$ is plotted as a function of m and r for various immune parameter values k and p_b under the growth-threshold assumption in Fig. 2 (the size-threshold analog is given by Fig. S2). A majority of recognition events occur

Recognition Mode	**Detection**	**Optimal growth strategy**
Deterministic (fixed)	Size-limited	$r > d$ only
Deterministic (fixed)	Growth-limited	$r > d$; $r < R/M$
Stochastic (adaptive)	Size-limited	$r > d$; $r \to d$
Stochastic (adaptive)	Growth-limited	$r > d$; $r \to R/M$ if $r < eR/M$; $r \to d$ if $r > eR/M$

Table S1: Static immune evasion strategies under various detection assumptions.

near $m = m_0$ when T-cell turnover rate is high and escape probability is low. Reductions in turnover k with preserved repertoire diversity (low p_b) therefore minimally affect immediate protection afforded to the host at the lower detection limit. Further immune compromise via increased p_b results in substantial impairment in immune recognition. Escape probability is approximated via Eq. S12 by

$$P_e = p_b \left(\frac{R}{rM} \right)^{k/r}. \tag{S24}$$

S4.2 Static threat summary

In all cases, one non-extinction strategy is extreme growth beyond the ability of immune elimination ($r > d$), which should be unrealistic for most invading threats. For deterministic recognition under size-limited detection, there is no alternative. Under deterministic, growth-limited detection there is a slow-growth window that permits immune escape. Such a situation applies to the innate immune system (Toll-like receptor and NK cell activation, for example) and supports the success of lysogenic viral infections or slow-growing, persistent intracellular bacteria [1, 2]. Under adaptive recognition, size-limited detection again favors threats with faster growth only, while growth-limited detection allows fast- or slow-growing threats to succeed. From a design perspective, growth-limited detection is an attractive system for targeting a rapidly growing pathogen, while sparing antigens that are expressed abundantly but not undergoing dramatic changes in their levels. These findings are summarized in Table S1.

S5 Dynamic threats

In this section, a dividing collection of initially detectable cells is capable of producing an immune evasive (type-2) subpopulation. As before, we characterize relevant growth strategies under the various assumptions outlined in the prior section. Here however, acquired immune evasion contributes to the survival strategy in addition to undetected escape to large sizes. A single immune evader must be produced prior to the elimination of type-1 cells in order for it to perpetuate the population. We therefore study the probability and mean arrival time of this first evader under the modeling assumptions listed previously.

In this case, a growing population may be sustained either by avoiding the immune system or by acquiring an immune evasive phenotype prior to extinction, which is assumed to occur at a per-cell rate of $\mu \ll 1$ per cell-division. Toward this end, we denote E_e to be the event that the dividing population escapes immune detection on $\{m_0, \dots, M\}$ and exceeds lethal size M. Similarly, we let E_μ denote the event that the threat successfully acquires an immune evader. Then all outcomes may be classified into one of four disjoint categories: 1. $E_{e,\mu^c} \equiv E_e \cap E_\mu^c$: Threat escape without type-2 population acquisition; 2. $E_{e,\mu} \equiv E_e \cap E_\mu$: Type-1 escape with type-2 population acquisition prior to detection; 3. $E_{e^c,\mu} \equiv E_e^c \cap E_\mu$: Type-1 recognition with type-2 acquisition prior to type-1 population extinction, and; 4. $E_{e^c,\mu^c} \equiv E_e^c \cap E_\mu^c$: Type-1 recognition without type-2 acquisition prior to type-1 population extinction. A dynamic threat is said ***to win*** if either E_e or $E_{e^c,\mu}$ occurs. A dynamic threat is said ***to lose*** if E_{e^c,μ^c} occurs. For notational convenience, we denote the probability of each of these events as follows:

$$P_e = \mathbb{P}(E_e); \qquad P_{e^c,\mu} = \mathbb{P}(E_{e^c,\mu}); \qquad P_l = \mathbb{P}(E_{e^c,\mu^c}). \tag{S25}$$

S5.1 Immune evasion arrival probability

We let τ_2 denote the time of type-2 population arrival and recall from Sec. S2 that S_1 (resp. $\tilde{S}_1$) is the time of type-1 detection (resp. extinction). Each immune threat starting at $X_1(0) = 1$ provides an opportunity for acquired immune evasion prior to threat recognition and subsequent elimination. The type-2 generation probability conditioned on immune recognition occurring at size $X_1 = m$, denoted by $P_{e^c,\mu}(m)$, is derived below. We will calculate this quantity by conditioning on the inter-arrival times $\Delta T_i = T_{i+1} - T_i$. It follows from the above dynamics that $\Delta T_i \sim \text{Exp}\big(ri - \mu ri\big)$.

Define N_i to be the number of (Poisson) arrivals of X_2 immune evaders on interval ΔT_i prior to immune recognition. Then N_i's distribution may be described by $\mathbb{P}\big(N_i = n\big) = (\mu ri \Delta T_i)^n e^{-\mu ri \Delta T_i}/n!$. Analogously, $\Delta \tilde{T}_i = \tilde{T}_{i-1} - \tilde{T}_i$, with $\Delta \tilde{T}_i \sim \text{Exp}\big(\tilde{r}i + \mu ri\big)$, with $\tilde{N}_i$ number of arrivals of X_2 evaders on $\Delta \tilde{T}_i$ having distribution given by $\mathbb{P}\big(\tilde{N}_i = n\big) = (\mu ri \Delta \tilde{T}_i)^n e^{-\mu ri \Delta \tilde{T}_i}/n!$.

Under net birth starting at size $X_1 = 1$ and up to $X_1 = m$ there are on average μ evaders produced per cell division, so we may estimate that there are $m - 1$ independent opportunities for X_2 generation, each with probability μ. Therefore, the probability that X_2 is acquired at least once on this birth trajectory is:

$$\mathbb{P}\big(\tau_2 < S_1 \;\big|\; X_1(S_1) = m\big) = 1 - (1 - \mu)^{m-1}. \tag{S26}$$

We remark that type-2 cell arrival prior to type-1 population recognition is rate-independent under the size-limited case (m_c), but not under growth-limited detection. We obtain $\mathbb{P}\big(S_1 \leq \tau_2 < \tilde{S}_1\big)$ below by conditioning on the exponentially distributed inter-arrival times:

$$
\begin{aligned}
\mathbb{P}\big(S_1 \le \tau_2 < \tilde{S}_1 \;\big|\; X_1(S_1) = m\big) &= \sum_{i=1}^{m-1} \mathbb{P}\big(\tilde{T}_i \le \tau_2 < \tilde{T}_{i-1}\big) \\
&= (1-\mu)^{m-1} \sum_{i=1}^{m} \prod_{j=i+1}^{m} \int_0^\infty e^{-\mu r j \tilde{t}_j} (\tilde{r} j + \mu r j) e^{-(\tilde{r} j + \mu r j)\tilde{t}_j} d\tilde{t}_j \\
&\cdot \int_0^\infty \big(1 - e^{-\mu r i \tilde{t}_i}\big)(\tilde{r} i + \mu r i) e^{-(\tilde{r} i + \mu r i)\tilde{t}_i} d\tilde{t}_i \\
&= (1-\mu)^{m-1} \sum_{i=1}^{m} \left(\prod_{j=i+1}^{m} \int_0^\infty (\tilde{r} + \mu r) j e^{-(\tilde{r} + 2\mu r) j \tilde{t}_j} d\tilde{t}_j \right) \\
&\cdot \int_0^\infty (\tilde{r} + \mu r) i \Big[e^{-(\tilde{r} + \mu r) i \tilde{t}_i} - e^{-(\tilde{r} + 2\mu r) i \tilde{t}_i} \Big] d\tilde{t}_i \\
&= (1-\mu)^{m-1} \sum_{i=1}^{m} \left(1 - \frac{\tilde{r} + \mu r}{\tilde{r} + 2\mu r}\right) \prod_{j=i+1}^{m} \left(\frac{\tilde{r} + \mu r}{\tilde{r} + 2\mu r}\right) \\
&= (1-\mu)^{m-1} \left(\frac{\mu r}{\tilde{r} + 2\mu r}\right) \sum_{i=1}^{m} \left(\frac{\tilde{r} + \mu r}{\tilde{r} + 2\mu r}\right)^{m-i} \\
&= (1-\mu)^{m-1} \left(\frac{\mu r}{\tilde{r} + 2\mu r}\right) \left(\frac{\tilde{r} + \mu r}{\tilde{r} + 2\mu r}\right)^{m} \sum_{i=1}^{m} \left(\frac{\tilde{r} + 2\mu r}{\tilde{r} + \mu r}\right)^{i} \\
&= (1-\mu)^{m-1} \left(\frac{\mu r}{\tilde{r} + 2\mu r}\right) \left(\frac{\tilde{r} + \mu r}{\tilde{r} + 2\mu r}\right)^{m} \left(\frac{\tilde{r} + 2\mu r}{\tilde{r} + \mu r}\right) \\
&\cdot \left(\frac{(\tilde{r} + \mu r)^m - (\tilde{r} + 2\mu r)^m}{(\tilde{r} + \mu r)^m}\right) \left(\frac{(\tilde{r} + \mu r)}{-\mu r}\right) \\
&= (1-\mu)^{m-1} \frac{(\tilde{r} + 2\mu r)^m - (\tilde{r} + \mu r)^m}{\big(\tilde{r} + 2\mu r\big)^m}. \qquad \text{(S27)}
\end{aligned}
$$

We have used the notational convention that $\prod_{j=1}^{0} f(j) = 1$ above. Thus, for $\tilde{r} > r$, we have that the type-2 generation probability conditioned on recognition at size $X_1 = m$, denoted by $P_{e^c,\mu}(m)$, is given by

$$
\begin{aligned}
P_{e^c,\mu}(m) &\equiv \mathbb{P}\big(\tau_2 < \tilde{S}_1 \;\big|\; X_1(S_1) = m\big) \\
&= \mathbb{P}\big(\tau_2 < S_1 \;\big|\; X_1(S_1) = m\big) + \mathbb{P}\big(S_1 \le \tau_2 < \tilde{S}_1 \;\big|\; X_1(S_1) = m\big) \\
&= 1 - (1-\mu)^{m-1} \left[1 - \frac{(\tilde{r} + 2\mu r)^m - (\tilde{r} + \mu r)^m}{\big(\tilde{r} + 2\mu r\big)^m}\right] \\
&= 1 - (1-\mu)^{m-1} \Big(\frac{\tilde{r} + \mu r}{\tilde{r} + 2\mu r}\Big)^m \\
&= 1 - (1-\mu)^{m-1} \left(\frac{d - (1-\mu) r}{d - (1-2\mu) r}\right)^m. \qquad \text{(S28)}
\end{aligned}
$$

S5.2 Mean arrival time of first immune evader

Even under the simpler, deterministic recognition assumption, type-2 arrival may not occur before extinction. We estimate T_μ, the expected first arrival time of type-2 cells conditioned on their arrival occurring prior to type-1 elimination, or, equivalently, on the event that $\tau_2 < \tilde{S}_1$. Members of X_2 arrive according to a non-homogeneous Poisson process with intensity given by $\lambda(t) = \mu r i$ on $t \in [T_i, T_{i+1}) \cup [\tilde{T}_i, \tilde{T}_{i-1})$. We wish to provide a mean estimate of τ_2 conditioned on the arrival of X_2 prior to extinction of population X_1

(otherwise $\tau_2 = \infty$). We will use mean values of birth (resp. death) arrival times, t_i (resp. $\tilde{t}_i$). The quantity of interest may be written as

$$T_\mu(m) \equiv \mathbb{E}\big[\tau_2 \,\big|\, \tau_2 < \tilde{S}_1\big]. \tag{S29}$$

Let I_F be the indicator function of event F. That is,

$$I_F = \begin{cases} 1 & \text{on } F, \\ 0 & \text{on } F^c. \end{cases} \tag{S30}$$

Let $E = [\tau_2 < \tilde{S}_1]$ denote the event that $\tau_2 < \tilde{S}_1$. Similarly, let $E_i = [t_i \le \tau_2 < t_{i+1}]$ and $\tilde{E}_i = [\tilde{t}_i \le \tau_2 < \tilde{t}_{i-1}]$ denote the events that time τ_2 occurs on interval $[t_i, t_{i+1})$ and $[\tilde{t}_i, \tilde{t}_{i-1})$, respectively. Then E is the disjoint union of $\{E_i\}_i$ and $\{\tilde{E}_i\}_i$. Therefore, by the definition of conditional expectation,

$$T_\mu(m) = \frac{\mathbb{E}[\tau_2 I_E]}{\mathbb{P}\big(\tau_2 < \tilde{S}_1\big)} = \Bigg(\sum_{i=1}^{m-1} \mathbb{E}\big[\tau_2 I_{E_i}\big] + \sum_{i=1}^{m} \mathbb{E}\big[\tau_2 I_{\tilde{E}_i}\big] \Bigg) \Big/ P_{e^c,\mu}(m), \tag{S31}$$

since $P_{e^c,\mu}(m) > 0$ (Equation S28). We will use Equation S31 to characterize mean immune evader arrival time. The arrival of type-2 cells during type-1 birth is an non-homogeneous Poisson process during mean time interval $[0, t_m)$, with intensity

$$\lambda(t) = \mu r i \quad \text{for} \quad t \in E_i \tag{S32}$$

and mean value function given by

$$m_\lambda(t) \equiv \int_0^t \lambda(\tau) d\tau. \tag{S33}$$

The time of first arrival has probability density

$$f(t) = \lambda(t) e^{-m_\lambda(t)}. \tag{S34}$$

Mean arrival times may be expressed as the sum of prior mean inter-arrivals:

$$t_{i+1} = \sum_{j=1}^{i} \Delta t_j = \sum_{j=1}^{i} \frac{1}{(1-\mu) r j} \approx h_i / r, \qquad \text{for } \mu \ll 1, \tag{S35}$$

where $h_i = \sum_{j=1}^{i} 1/j$ is the harmonic series. Thus, for $t \in [t_i, t_{i+1})$,

$$\begin{aligned} m_\lambda(t) &= \int_0^{t_i} \lambda(\tau) d\tau + \int_{t_i}^{t} \lambda(\tau) d\tau \\ &= \sum_{j=1}^{i-1} \mu r j (t_{j+1} - t_j) + \int_{t_i}^{t} \mu r i d\tau \\ &\approx \sum_{j=1}^{i-1} \mu r j \Big(h_j - h_{j-1} \Big) / r + \mu r i t - \mu r i t_i \\ &= \sum_{j=1}^{i-1} \mu + \mu r i t - \mu i h_{i-1} \\ &= \mu \big(i - 1 - i h_{i-1} \big) + \mu r i t. \end{aligned} \tag{S36}$$

Therefore,

$$f(t) \approx \mu r i e^{-\mu(i-1-ih_{i-1})} e^{-\mu r i t}. \tag{S37}$$

Thus we may write

$$\begin{aligned}
\mathbb{E}[\tau_2 I_{E_i}] &= \int_{t_i}^{t_{i+1}} t f(t) dt \\
&\approx e^{-\mu(i-1-ih_{i-1})} \int_{t_i}^{t_{i+1}} t\mu r i e^{-\mu r i t} dt \\
&= e^{-\mu(i-1-ih_{i-1})} \Big(\Big[-te^{-\mu r i t} \Big]_{t=t_i}^{t_{i+1}} + \int_{t_i}^{t_{i+1}} e^{-\mu r i t} dt \Big) \\
&= e^{-\mu(i-1-ih_{i-1})} \Big\{ \Big(t_i + \frac{1}{\mu r i} \Big) e^{-\mu r i t_i} - \Big(t_{i+1} + \frac{1}{\mu r i} \Big) e^{-\mu r i t_{i+1}} \Big\} \\
&\approx e^{-\mu(i-1-ih_{i-1})} \Big\{ \Big(\frac{h_{i-1}}{r} + \frac{1}{\mu r i} \Big) e^{-\mu i h_{i-1}} - \Big(\frac{h_i}{r} + \frac{1}{\mu r i} \Big) e^{-\mu i h_i} \Big\} \\
&= \Big(\frac{h_{i-1}}{r} + \frac{1}{\mu r i} \Big) e^{-\mu(i-1)} - \Big(\frac{h_i}{r} + \frac{1}{\mu r i} \Big) e^{-\mu i} \\
&= \frac{1}{r} \Big[h_{i-1} e^{-\mu(i-1)} - h_i e^{-\mu i} + \frac{1}{\mu i} \big(e^{-\mu(i-1)} - e^{-\mu i} \big) \Big].
\end{aligned} \tag{S38}$$

Summing over E_i, we have,

$$\begin{aligned}
\sum_{i=1}^{m-1} \mathbb{E}[\tau_2 I_{E_i}] &= \frac{1}{r} \Bigg(\sum_{i=1}^{m-1} \Big(h_{i-1} e^{-\mu(i-1)} - h_i e^{-\mu i} \Big) + \sum_{i=1}^{m-1} \frac{1}{\mu i} \big(e^{-\mu(i-1)} - e^{-\mu i} \big) \Bigg) \\
&= \frac{1}{r} \Bigg(-e^{-\mu(m-1)} \sum_{i=1}^{m-1} \frac{1}{i} + \sum_{i=1}^{m-1} \frac{1}{\mu i} \big(e^{-\mu(i-1)} - e^{-\mu i} \big) \Bigg) \\
&= \frac{1}{r} \sum_{i=1}^{m-1} \frac{1}{i} \Big[\frac{1}{\mu} \big(e^{-\mu(i-1)} - e^{-\mu i} \big) - e^{-\mu(m-1)} \Big]
\end{aligned} \tag{S39}$$

Expanding $\frac{1}{\mu}\big(e^{-\mu(i-1)} - e^{-\mu i}\big) - e^{-\mu(m-1)}$ at $\mu = 0$ and approximating by the linear term in μ yields

$$\begin{aligned}
&\approx \frac{1}{r} \sum_{i=1}^{m-1} \frac{1}{i} (m - i + 1/2)\mu \\
&= \frac{\mu}{r} \Big[(m + 1/2) h_{m-1} - (m-1) \Big] \\
&\approx \frac{m}{r} \Big(\log m - 1 \Big) \mu.
\end{aligned} \tag{S40}$$

We note that

$$\frac{m}{r} \Big(h_{m-1} - 1 \Big) \mu < h_{m-1}/r = E[T_1], \qquad \text{for } \mu m < 1,$$

the above inequality holding whenever $\mu m < 1$.

We may provide an estimate for $\mathbb{E}[\tau_2 I_{\tilde{E}}]$ by similar approach. Recall that $\tilde{t}_i$ denotes the mean time that the population decreases to size i, and $\Delta\tilde{t}_i$ its respective mean inter-arrival time. Let $\tilde{h}_j = \sum_{k=j}^{m} 1/k$. Then $\tilde{t}_m = t_m$ and

$$\tilde{s}_i = t_m + \frac{1}{\mu r + \tilde{r}} \tilde{h}_{i+1} \approx t_m + \tilde{h}_{i+1}/\tilde{r} \qquad \text{for } \mu \ll 1. \tag{S41}$$

Additionally, $\lambda(t) = \mu r i$ and $f(t) = \lambda(t)e^{-m_\lambda(t)}$ on $\tilde{E}_i = [\tilde{t}_i, \tilde{t}_{i-1})$, with

$$\begin{aligned}
m_\lambda(t) &= \int_0^t \lambda(\tau)d\tau \\
&= \int_0^{t_{m-1}} \lambda(\tau)d\tau + \int_{\tilde{t}_m}^{\tilde{t}_i} \lambda(\tau)d\tau + \int_{\tilde{t}_i}^{t} \lambda(\tau)d\tau \\
&= \sum_{j=1}^{m-1} \mu r j(t_{j+1} - t_j) + \sum_{j=i}^{m} \mu r j(\tilde{t}_{j-1} - \tilde{t}_j) + \int_{\tilde{t}_i}^{t} \mu r i d\tau \\
&\approx \mu \sum_{j=1}^{m-1} j\Big(h_j - h_{j-1}\Big) + \frac{\mu r}{\tilde{r}} \sum_{j=i}^{m} j\Big(\tilde{h}_j - \tilde{h}_{j+1}\Big) + \mu r i(t - \tilde{t}_i) \\
&= \mu(m-1) + \frac{\mu r}{\tilde{r}}(m - i + 1) - \mu r i\tilde{t}_i + \mu r i t \\
&\approx \frac{\mu}{\tilde{r}} m(\tilde{r} - r) - \frac{\mu r}{\tilde{r}} i - \mu r i\tilde{t}_i + \mu r i t, \qquad \text{for } m \gg 1 \\
&\equiv C_i + \mu r i t.
\end{aligned}$$

Therefore,

$$\begin{aligned}
\mathbb{E}\big[\tau_2 I_{\tilde{E}_i}\big] &= \int_{\tilde{t}_i}^{\tilde{t}_{i-1}} t f(t) dt \\
&\approx \int_{\tilde{t}_i}^{\tilde{t}_{i-1}} \mu r i t e^{-C_i} e^{-\mu r i t} dt \\
&= e^{-C_i}\Big[\tilde{t}_i e^{-\mu r i \tilde{t}_i} - \tilde{t}_{i-1} e^{-\mu r i \tilde{t}_{i-1}} + \frac{1}{\mu r i}(e^{-\mu r i \tilde{t}_i} - e^{-\mu r i \tilde{t}_{i-1}})\Big] \\
&\approx e^{-\frac{\mu}{\tilde{r}} m(\tilde{r}-r) + \frac{\mu r}{\tilde{r}} i + \mu r i \tilde{t}_i}\Big[e^{-\mu r i \tilde{t}_i}\Big(\tilde{t}_i - \tilde{t}_{i-1} e^{-\frac{\mu r}{\tilde{r}}} + \frac{1}{\mu r i}\big(1 - e^{-\frac{\mu r}{\tilde{r}}}\big)\Big)\Big] \\
&= e^{-\frac{\mu}{\tilde{r}} m(\tilde{r}-r)} e^{\frac{\mu r}{\tilde{r}} i}\Big[\tilde{t}_i - \tilde{t}_{i-1} e^{-\frac{\mu r}{\tilde{r}}} + \frac{1}{\mu r i}\big(1 - e^{-\frac{\mu r}{\tilde{r}}}\big)\Big].
\end{aligned} \tag{S42}$$

Summing over $\tilde{E}_i$, we have,

$$\begin{aligned}
\mathbb{E}[\tau_2 I_{\tilde{E}}] &= \sum_{i=1}^{m} \mathbb{E}[\tau_2 I_{\tilde{E}_i}] \\
&\approx e^{-\frac{\mu}{\tilde{r}} m(\tilde{r}-r)} \sum_{i=1}^{m} \left(\tilde{t}_i e^{\frac{\mu r}{\tilde{r}} i} - \tilde{t}_{i-1} e^{\frac{\mu r}{\tilde{r}}(i-1)} + \frac{1 - e^{-\frac{\mu r}{\tilde{r}}}}{\mu r i} e^{\frac{\mu r}{\tilde{r}} i}\right) \\
&= e^{-\frac{\mu}{\tilde{r}} m(\tilde{r}-r)} \left(\tilde{t}_m e^{\frac{\mu r m}{\tilde{r}}} - \tilde{t}_0 + \sum_{i=1}^{m} \frac{e^{\frac{\mu r}{\tilde{r}} i} - e^{\frac{\mu r}{\tilde{r}}(i-1)}}{\mu r i}\right) \\
&= e^{-\frac{\mu}{\tilde{r}} m(\tilde{r}-r)} \left(\frac{h_{m-1}}{r} e^{\frac{\mu r m}{\tilde{r}}} - \frac{h_{m-1}}{r} - \frac{\tilde{h}_1}{\tilde{r}} + \sum_{i=1}^{m} \frac{e^{\frac{\mu r}{\tilde{r}} i} - e^{\frac{\mu r}{\tilde{r}}(i-1)}}{\mu r i}\right) \\
&= e^{-\frac{\mu}{\tilde{r}} m(\tilde{r}-r)} \left(\frac{h_{m-1}}{r}\big(e^{\frac{\mu r m}{\tilde{r}}} - 1\big) - \frac{h_m}{\tilde{r}} + \frac{1}{\tilde{r}} \sum_{i=1}^{m} \frac{1}{i} \frac{e^{\frac{\mu r}{\tilde{r}} i} - e^{\frac{\mu r}{\tilde{r}}(i-1)}}{\mu r/\tilde{r}}\right) \\
&= e^{-\frac{\mu}{\tilde{r}} m(\tilde{r}-r)} \left[\frac{h_{m-1}}{r}\big(e^{\frac{\mu r m}{\tilde{r}}} - 1\big) + \frac{1}{\tilde{r}} \sum_{i=1}^{m} \frac{1}{i}\left(\frac{e^{\frac{\mu r}{\tilde{r}} i} - e^{\frac{\mu r}{\tilde{r}}(i-1)}}{\mu r/\tilde{r}} - 1\right)\right].
\end{aligned}$$

Taking the Taylor expansions of $e^{-\frac{\mu}{\tilde{r}}m(\tilde{r}-r)}\big(e^{\frac{\mu r m}{\tilde{r}}}-1\big)$ and $e^{-\frac{\mu}{\tilde{r}}m(\tilde{r}-r)}\big(\frac{e^{\frac{\mu r}{\tilde{r}}i}-e^{\frac{\mu r}{\tilde{r}}(i-1)}}{\mu r/\tilde{r}}-1\big)$, we obtain to first order in μ,

$$\begin{aligned}\mathbb{E}[\tau_2 I_{\tilde{E}}] &\approx \frac{1}{r}h_{m-1}\frac{mr}{\tilde{r}}\mu+\frac{1}{\tilde{r}}\Big(\frac{r}{\tilde{r}}\Big)\Big(m-\frac{h_m}{2}\Big)\mu\\ &\approx \Big(\frac{r}{\tilde{r}}\Big)\Big(\frac{m}{r}\log m+\frac{m}{\tilde{r}}-\frac{1}{2\tilde{r}}\log m\Big)\mu\\ &= \Big(\frac{r}{d-r}\Big)\Big(\frac{m}{r}\log m+\frac{m}{d-r}-\frac{1}{2(d-r)}\log m\Big)\mu. \end{aligned} \tag{S43}$$

Thus,

$$\mathbb{E}[\tau_2 I_E] \approx \Big[\frac{m}{r}\Big(\log m-1\Big)+\Big(\frac{r}{d-r}\Big)\Big(\frac{m}{r}\log m+\frac{m}{d-r}-\frac{1}{2(d-r)}\log m\Big)\Big]\mu, \tag{S44}$$

and so

$$T_\mu(m) \approx \mu\Big[\frac{m}{r}\Big(\log m-1\Big)+\Big(\frac{r}{d-r}\Big)\Big(\frac{m}{r}\log m+\frac{m}{d-r}-\frac{1}{2(d-r)}\log m\Big)\Big]/P_{e^c,\mu}(m) \tag{S45}$$

follows by applying Eqs. S28 and S44 to Eq. S31. Agreement between simulations and our analytic theory can be seen in Fig. S3 (see more detail below). From this, we find that the acquisition of immune evaders for extreme values of r are more likely and, on average, arrive after a larger amount of time. For intermediate growth rates where evader generation is rare (Eq. S28), type-2 arrivals, if they occur, must necessarily appear quickly. Moreover, the output for reasonable parameter choice suggests that in contrast to evader generation probability, mean evader arrival time may be less helpful for differentiating between growth-limited vs. size-limited recognition modes (Fig. 3).

S5.3 Growth strategies for dynamic threats

As in the static case, a dynamic threat succeeds if it successfully avoids detection and grows past size M. Dynamic threats also have the ability to succeed if they can create an immune evader prior to elimination. Successful growth beyond M follows exactly the same behavior as in the static case since the presence or absence of type-2 cells does not affect the outcome.

S5.3.1 Deterministic recognition

Since immune detection occurs with certainty, we have that

$$P_{e^c,\mu} = P_{e^c,\mu}(m_0); \tag{S46}$$

$$P_e = 0; \tag{S47}$$

$$P_l = 1-P_{e^c,\mu}(m_0). \tag{S48}$$

Thus threat escape depends solely upon the production of a type-2 cell prior to type-1 extinction, so it suffices to only consider $P_{e^c,\mu}$ under deterministic recognition[1].

Size-limited detection: Here, both $P_{e^c,\mu}$ and T_μ may be analyzed by substituting $m=m_c$ directly into Eqs. S28 and S45. Agreement between theory and simulations is illustrated in Fig. S3A,B. From this, we find that type-2 generation probability is an increasing function of net growth rate. Mean arrival time is large for both small r and large r. The former case is due to a larger average time until first immune evader arrival, while the latter occurs by virtue of the fact that a majority of evaders arrive during the long time interval of net-death prior to elimination (Eq. S4). Together, this suggests that for size-limited detection, immune evaders rarely occur for slow-growing threats and only do so on average over a long time period.

[1]Note that $P_e=0$ implies that E_e is a $\mathbb{P}$-null set, and so $\mathbb{P}(E_\mu)=\mathbb{P}(E_\mu\cap E_e)+\mathbb{P}(E_\mu\cap E_e^c)=P_{e^c,\mu}$ follows directly from $(E_\mu\cap E_e)\subseteq E_e$.

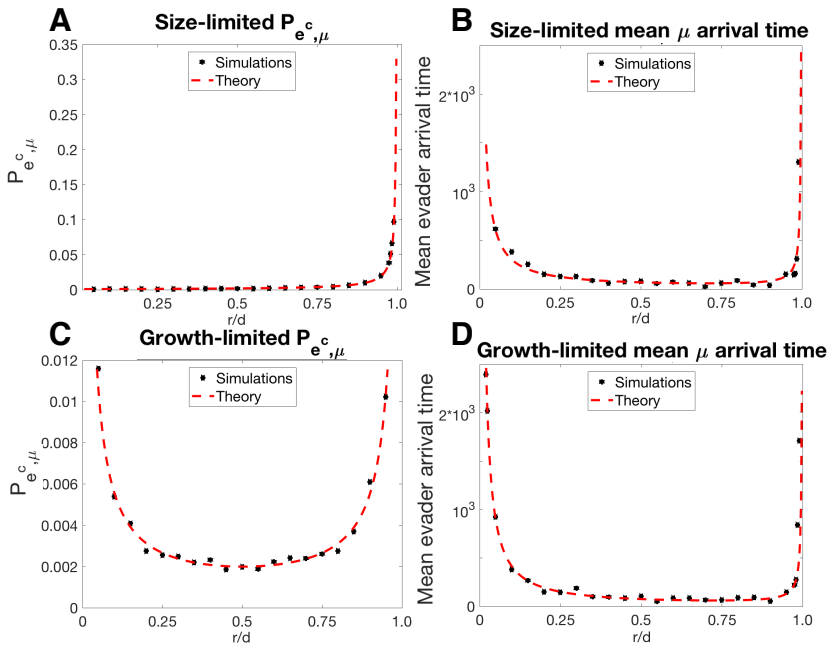

Figure S3: Simulations vs theory for evader arrival probabilities and mean arrival times. (A) Immune evader arrival probability, $P_{e^c,\mu}$, and (B) mean time of evader arrival, T_μ, for size-limited detection; ($m_0 = 10^3$); (C) $P_{e^c,\mu}$ and (D) T_μ for growth-limited detection; $R = 100$ (in all cases, $d = 0.2$, $\mu = 10^{-6}$, with averages over $5 \cdot 10^4$ simulations).

Growth-limited detection: In a similar strategy as above, substitution of $m_0(r) = \lceil R/r \rceil$ into Eqs. S28 and S45 give analytical probability and mean evader arrival time. These results are plotted alongside simulations in Fig. S3C,D. In contrast with the predictions for size-limited detection, type-2 generation probability is maximal for large *and* small values of r relative to d. Moreover, the time scales of type-2 acquisition for both fast and slow growth threats are comparable. This is because threats with r approaching d are recognized at small population sizes, but can maintain their size over a longer period of time due to low net death rates. Conversely, r approaching 0 enables a population to reach larger sizes before being recognized and quickly eliminated. One implication of this is that the risk of type-2 arrival will never be entirely eliminated by enhancement of immune killing ability (via increased d) alone, and such an immune modulation is predicted to have a weaker effect at controlling slow-growth threats that are more likely to acquire an evasive phenotype prior to immune killing. This analysis characterizes immune recognition behavior in the limit of small escape probability $p_e \to 0$ so that all threats are recognized once reaching detection size, which is applicable to setting of memory immunity against a previously encountered threat.

S5.3.2 Adaptive immune recognition

This is the most involved, and arguably relevant, setting for studying the behavior of cancer-immune dynamics. Here, recognition may occur randomly for $X = m \in \{m_0, m_0 + 1, \cdots, M\}$. We may find $P_{e^c,\mu}$ in this case by considering the probability $P_{e^c,\mu}(m)$ of immune evader arrival conditioned on detection at size

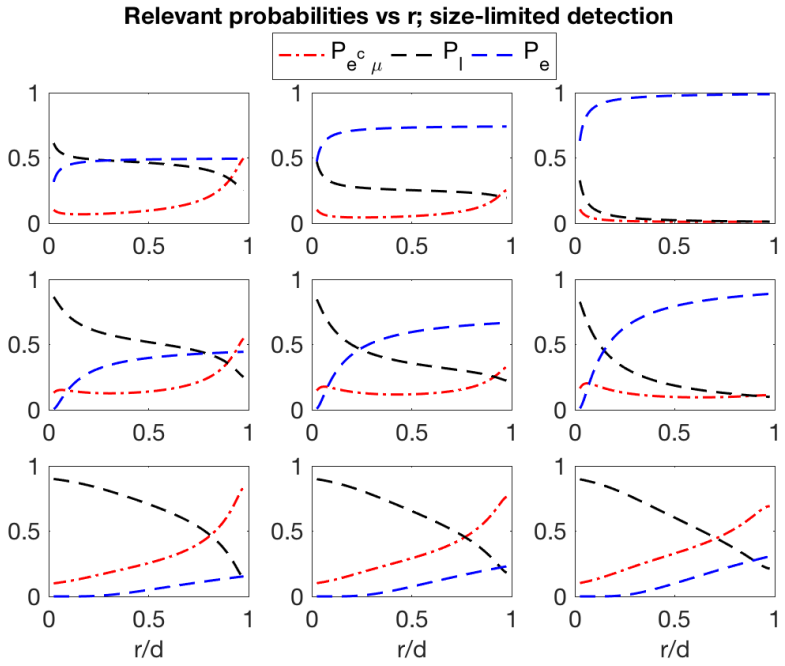

Figure S4: Size-limited, dynamic threat escape, evasion, and loss probabilities. Dynamic threat escape, evasion, and loss probabilities as a function of relative net growth rate r/d for various values of immune turnover (rows bottom-to-top: k=$\{10^{-1}, 10^{-2}, 10^{-3}\}$) and repertoire diversity (columns left-to-right: p_b=$\{0.5, 0.75, 1.0\}$) ($d = 0.20$, $\mu = 10^{-6}$, $m_c = 10^5$, $M = 10^6$).

m via Eqs. S15, S28. The three probabilities of interest are given by:

$$P_{e^c,\mu} = P_{e^c,\mu}(m_0 \leq m \leq M) = I_{[m_0<M]} \sum_{m=m_0}^{M} P_{e^c,\mu}(m) \cdot p_r(m; m_0), \tag{S49}$$

$$P_e = p_e(M; m_0) \approx p_b \big(m_0/M\big)^{k/r}, \tag{S50}$$

$$P_l = P_l(m_0 \leq m \leq M) = 1 - (P_{e^c,\mu} + P_e). \tag{S51}$$

Size-limited detection: Relevant probabilities may be calculated using Eqs. S49-S51 with $m_0 = m_c$ and are depicted in Fig. S4. In this case, the probability of immune victory decreases for increasing growth rates over a wide variety of immune turnover rates and repertoire diversity. This continues the theme of preferred large growth threats seen in analysis of the static, size-limited case.

Growth-limited detection: As above, we can make use of Eqs. S49-S51 using $m_0 = m_0(r)$, keeping in mind that recognition only occurs for r such that $m_0(r) < M$. Plots of the analytical probability estimates are given for several selections of immune parameters p_b and k in Fig. 4. It is evident in this case that a variety of behaviors for the likelihood of escape and immune evasion depend on the relative choice of k and p_b. We observe that under high immune turnover and repertoire diversity (high k and low p_b) immune detection failure stems primarily from acquired immune evasion. As immune turnover rate and repertoire diversity is compromised, immune escape dominates in the overall contribution to the probability of a dynamic threat victory. In contrast to the size-limited case, dynamic threats under growth-limited detection enjoy increased chances of victory for large and small growth rates, and, under a critical limit, threats can sneak-through immune detection.

S5.4 Dynamic threat summary

Dynamic threats are considered successful if they either escape immune detection, as in the case of a static threat, or acquire a type-2 cell despite recognition prior to elimination. When recognition is deterministic, the latter event is the only path to victory. When detection is size-limited, rapidly growing threats succeed exclusively. Growth-limited detection allows both fast and slow growing threats to succeed via immune evasion. Under adaptive immune recognition, the optimal strategy depends on immune turnover and background recognition rates. In the growth-limited case, preferential success of slow and rapidly growing threats is seen when there is minimal immune compromise. Threat victory under various reductions in immune turnover and repertoire size depends on the nature of immune compromise. Dynamic threat optimal growth strategies share some similarities with those of static threats, although the advantage of a slower growth rate is more pronounced for a dynamic threat owing to its ability to acquire immune evaders prior to detection. These strategies are summarized in Table S2.

Recognition Mode	**Detection**	**Optimal growth strategy**
Deterministic (fixed)	Size-limited	$r > d$; r large for maximal $P_{e^c,\mu}$
Deterministic (fixed)	Growth-limited	$r > d$; $r \to d$ or $r \to R/M$ for maximal $P_{e^c,\mu}$
Stochastic (adaptive)	Size-limited	$r > d$; $r \to d$ for maximal $P_{e^c,\mu}$; $P_e = P_e(p_b, k)$
Stochastic (adaptive)	Growth-limited	$r > d$; $r \to d$ or $r \to R/M$ for maximal $P_{e^c,\mu}$; $P_e = P_e(p_b, k)$

Table S2: Dynamic threat immune evasion strategies under various detection assumptions.

S6 Predicted effects of decreased thymic output recognition

The analytic results of the prior section would suggest that cancer incidence, occurring either as a result of acquired immune evasion or population escape, depends to a large degree on the state of the adaptive immune compartment. Motivated by this, we apply our foundational model to make a simplified prediction of cancer incidence as a function of an aging immune compartment. We select AML as a prototypical example, due to its low mutational burden in addition to the fact that adequate T-cell infiltration and any additional inhibitory effects of the tumor microenvironment are less of a concern in hematological malignancies. It is known that thymic output decreases exponentially as a function of age by over 95% from age 25-60 with initial preservation of T-cell diversity [3]. T-cell diversity is compromised in advanced age and decreases 100-fold by age 75. These concepts can conveniently be decoupled in the framework above since repertoire diversity is related to the total number of distinct immune cell clones, which in turn is related to p_b, while turnover is related to k.

We assume equal risk across all ages of AML founder arrival sensitive to initial immune targeting and neglect more subtle fitness changes imparted by driver and passenger mutations, an assumption mitigated by the low mutational burden of AML. Thymic turnover k is modeled as a Hill function that decreases two orders of magnitude ($k = 1$ to $k = 10^{-2}$) centered at age 20 (Fig. S5A). The probability, $\tilde{p}$, that an individual TCR recognizes tumor antigenic peptide is estimated at $\tilde{p} \sim 10^{-6}$ as characterized previously in [4]. The Immune repertoire diversity, represented by the total number of effective T-cell clones, N_t, is assumed to decrease two orders of magnitude ($N_t = 2.5 \cdot 10^6$ to $N_t = 2.5 \cdot 10^4$) centered at age 67 (Fig. S5B). In each case, Hill coefficients were selected to emulate the assumed immune profile. The background escape probability may be calculated using the total repertoire diversity via $p_b = (1 - \tilde{p})^{N_t}$, as done previously [4] (Fig. S5C). As before, we fix $d = 0.20$, and approximate $r \sim d/10$ for AML so that the growth rate is definitively below the maximal immune targeting rate. We estimate $\mu \sim 10^{-9}$ to represent the rate of rare arrivals of immune-evasive phenotypes. We expect μ to be no larger than this, but found that this parameter most influenced incidence in early age and this order of magnitude estimate best characterized early age incidence (described below). We take $M \sim 10^6$ and $R = 10^2$ so that $m_0(r) = 5000$. Using these functional forms, we calculate escape, P_e, and evasion, $P_{e^c,\mu}$, comparing these predictions to age-related incidence (Fig. S6). Gender-specific differences exist between male and female thymic output as well as AML incidence [5], and although we do not model this here, the relative reduction in female relative to male incidence coincides with greater immune functioning in females and further reinforces the postulate that adequate immune functioning plays a crucial role in controlling tumor incidence. We also compare this model to the multi-stage theory of incidence that assumes increased risk proportional to a power of age [6, 7] for various numbers of 'hits'. We demonstrate overall better agreement in our model for the parameters selected above when compared to the best fit versions of each multi-stage model (Fig. 5A).

The comparison of our analytical estimate against empirical data suggests that AML incidence can be divided into three parts: minimal cases of early disease due to the rare arrival of type-2 cells that escape immune detection, a slight increase in incidence during middle age due to increased risk secondary to lower turnover rates, and late-onset disease as a result of decreasing TCR repertoire diversity. In light of uncertainty regarding the true parameter values for AML, we remark that the estimates given above are most sensitive to the underlying cancer immune evasion rate μ, and in fact μ dominates the predicted disease incidence during young ages, but contributes less to the behavior at larger ages. Once selected, the curve was optimized by a parameter search for the order of magnitude of m_0 and M, resulting in good general agreement for a reasonable selections of detection and incidence sizes. Changes to these parameters affect the predicted tumor escape probabilities, with the escape probability varying directly (resp. inversely) with m_0 (resp. M). Perturbations to the assumed ending values for normalized T-cell turnover and repertoire diversity have the largest effect on predicted escape probabilities in advanced age. Changes in the Hill coefficients which resulted in similar immune turnover and repertoire diversity profiles had a minimal effect on the overall predictions.

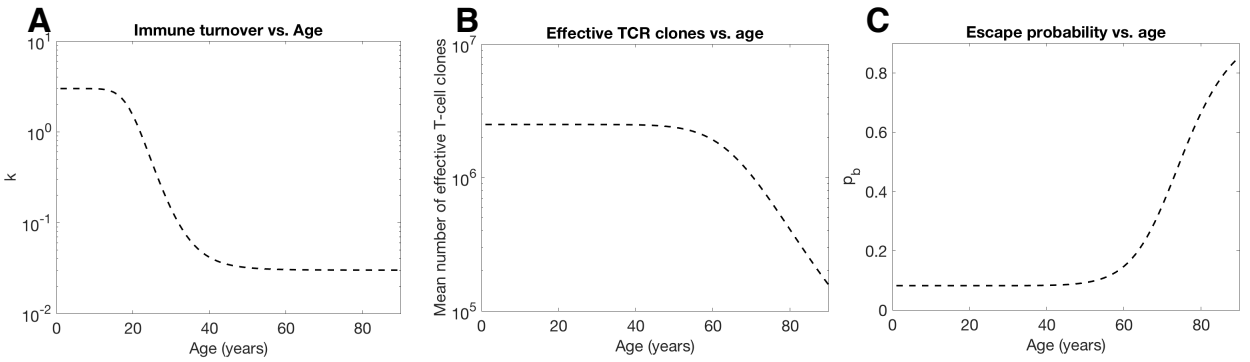

Figure S5: Constitutive relations for AML incidence curve. (A) Immune turnover (k) vs. age (t) is assumed to follow $k(t) = k_0 - (k_0 - k_f)t^{n_k}/(K_k^{n_k} + t^{n_k})$ (graphed for $k_0 = 3$, $k_f = 3 \cdot 10^{-2}$, $n_k = 8$); (B) Number of effective TCR clones (N_t) vs. age (t) is assumed to follow $N_t = N_0 - (N_0 - N_f)t^{n_N}/(K_N^{n_N} + t^{n_N})$; (graphed for $N_0 = 2.5{\cdot}10^6$, $N_f = 2.5{\cdot}10^4$, $n_N = 10$) ; (C) Escape probability ($p_b(t)$) vs. age is calculated using number of effective clones and the probability $\tilde{p}$ of a single clone recognizing tumor antigen as $p_b(t) = 1 - p_c(t)$, where $p_c(t) = 1 - (1 - \tilde{p})^{N_t}$ (graphed for $\tilde{p} \sim 10^{-6}$).

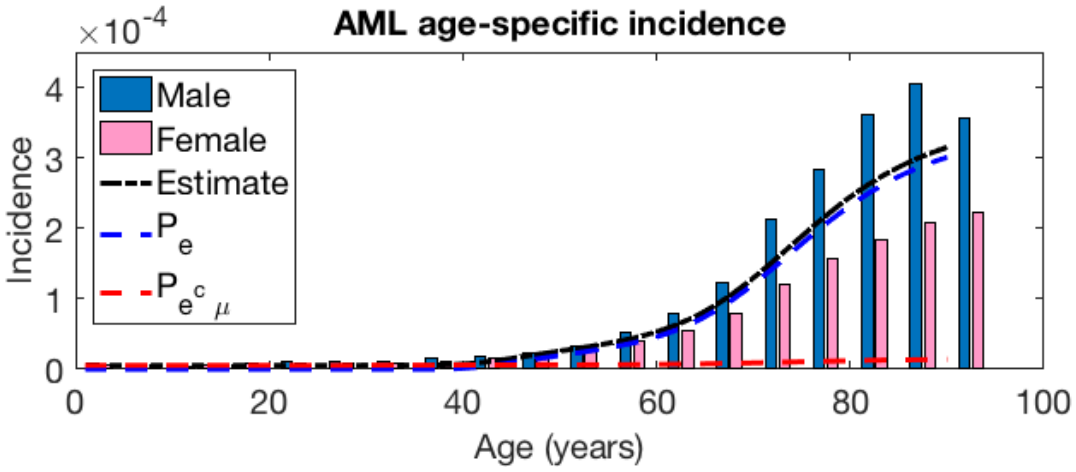

Figure S6: AML age and gender-specific incidence. Bar plot of empirical data is compared to model-derived AML estimates $P_e + P_{e^c,\mu}$ that assumes constant cancer incidence and decreasing immunity vs age.

Our analysis suggests a correlation between age and AML incidence is explained partly by immune performance and would suggest that an attempt be made to maximize thymic output and T-cell diversity in middle and advanced age to minimize the likelihood of AML incidence. For patients with chemotherapy-refractory AML, often treated with allogeneic stem cell therapy, the clinical focus should be on maximizing repertoire diversity and thymic output post-transplant. More generally, efforts to mitigate cancer occurrence should focus on maximizing immune repertoire diversity shortly after treatment [8].

Motivated by this observation, we argued by similar reasoning that long-term immunosuppression of the adaptive immune compartment might manifest in increased cancer occurrence. In order to test this, we kept all relevant parameters for AML fixed at their values in the previous investigation, and evaluated the predicted effect of mild, chronic CD8+ T-cell immunosuppression commonly imposed post-transplant on longterm

AML incidence. We assumed immunosuppression mildly inhibits both current and future repertoires so that the new recognition probability $1 - p_b$ and effective turnover rate k are scaled by $\alpha = 0.90$. We considered 10-year cumulative AML incidence assuming equal risk across age groups. Our estimates predict a significant increase in cumulative AML incidence (Fig. 5B) and are in general agreement with empirical observations for transplant patients under chronic immunosuppression [9], further highlighting the importance of proper immune functioning in disease prevention.

S7 Predicted effects of immunotherapy

S7.1 Detection

Here we provide the general framework for quantifying treatment success probabilities for Chimeric antigen receptor (CAR) T-cell and antigen vaccine immunotherapeutic strategies. We assume that adjuvant immunotherapy is given following initial ablative chemotherapy or radiation to reduce tumor burden. Treatment is administered at detection time T_D when $X_1(T_D) + X_2(T_D) = M$, and assumed to quickly reduce tumor size to minimal residual disease size $X_1(T_D+) + X_2(T_D+) = m_{mrd} \ll M$. The time for treatment is assumed small compared to the progression of the initial disease so that we may neglect the possibility of type-2 cells arriving on the therapy interval. All therapies described below are assumed to occur after tumor reduction via this treatment.

We define the event, E of overall disease elimination. In all cases, the cancer population is modeled as an adaptive threat. Individuals presenting with disease do so only if the threat is victorious, which we recall from Section S5 occurs if either E_e or $E_{e^c,\mu}$ occurs. The population escapes with type-2 acquisition prior to detection on $E_{e,\mu}$ with probability $P_{e,\mu}$, and the population escapes without type-2 acquisition prior to detection on E_{e,μ^c} with probability P_{e,μ^c}. The overall disease elimination probability may be factored using the law of total probability, giving

$$P_E \equiv P_T + P_l, \tag{S52}$$

for

$$P_T \equiv \mathbb{P}\big(E \mid E_{e,\mu}\big)P_{e,\mu} + \mathbb{P}\big(E \mid E_{e,\mu^c}\big)P_{e,\mu^c} + \mathbb{P}\big(E \mid E_{e^c,\mu}\big)P_{e^c,\mu}. \tag{S53}$$

We make the slight distinction above between disease elimination prior to treatment (P_l), treatment elimination (P_E), and overall disease elimination probability (P_E). Eq. S53 will be applied to quantify the immunotherapy strategies investigated below.

S7.2 CAR T-cell therapy

CAR T-cells are a class of *ex-vivo* engineered T-cells with artificial T-cell receptors (TCRs) designed to target an epitope differentially present on cancer cells [10]. Variations and improvements, such as high-affinity MHC-derived CARs as well as co-stimulatory signaling, have enhanced the functionality of these therapies, particularly in solid tumors that, unlike their hematological counterparts, often lack co-stimulatory molecules [11, 12]. Importantly, the CAR T-cell receptor is not limited to MHC-I recognition and can recognize a number of preferentially expressed tumor cell signatures, including surface proteins and carbohydrates [13]. CAR T-cell therapy has been successful in treating a number of malignancies, including treatment refractory acute lymphoblastic leukemia, where mutation burden (and therefore tumor neoantigen availability) is low [14, 15]. Their success in solid malignancies requires selection of preferentially over-expressed tumor-specific antigens in the bulk tumor [16, 17].

Our analysis considers the case where identification of such tumor-specific CARs has been obtained. In contrast to the entire immune repertoire problem considered earlier, a clonal CAR T-cell population is introduced against a specific surface epitope following chemoablative therapy. We assume CAR T-cell co-stimulatory signaling circumvents the conventional immune detection limit following its initial epitope encounter, so that detection occurs deterministically at some size m_{car} following ablative therapy. For simplicity, we assume that $m_{car} \leq m_{mrd}$ for some sufficiently large but fixed dosage of CAR T-cells so that detection occurs immediately at size m_{mrd}, but the following approach is general enough to handle the opposite case ($m_{mrd} < m_{car}$) with minimal modification. In this case, E represents the event that CAR T-cells, engineered against a ubiquitous target expressed on the current cancer cell population, recognize and eliminate the threat. We allow for the potential emergence of a CAR T-cell evasive phenotype, which

may in general arrive at rate μ_{car} distinct from general TCR evasion rate μ. We neglect the rare event that an epitope-evasive clone is present prior to treatment, given the lack of fitness advantage for such a threat prior to therapy.

Under the above dynamics, E occurs with the same probability regardless of the history prior to detection time, since all cells are assumed detectable immediately following treatment at time T_D+. Moreover, recognition occurs deterministically at size m_{mrd}, so that $P_e = 0$ which implies that $P_\mu = P_{e^c,\mu}$. Thus, all three of the conditional success probabilities, $\mathbb{P}(E|\,\cdot\,)$, in Eq. S53 reduce to the deterministic recognition case with detection limit m_{mrd} and post-treatment starting size m_{mrd}, so that

$$\mathbb{P}\big(E \mid E_{e,\mu^c}\big) = \mathbb{P}\big(E \mid E_{e,\mu}\big) = \mathbb{P}\big(E \mid E_{e^c,\mu}\big) = P_{\mu^c} = 1 - P_{e^c,\mu}\big(m_{mrd}; m_{mrd}\big). \tag{S54}$$

Here, we introduce some slight modifications to Eq. S28 to account for a process starting at $X(T_D+) = m_{mrd}$, deterministically recognized at $m \geq m_{mrd}$, and perhaps having a distinct evasion rate μ_{car} dependent upon the CAR T-cell target. We denote this modification by $P_{e^c,\mu}(m; m_{mrd})$, which takes the form

$$P_{e^c,\mu}(m; m_{mrd}) \equiv P_{e^c,\mu}\big(m \mid X(T_D+) = m_{mrd}\big) = 1 - (1-\mu_{car})^{m-m_{mrd}} \left(\frac{d-(1-\mu_{car})r}{d-(1-2\mu_{car})r}\right)^{m_{mrd}}. \tag{S55}$$

Thus, in the CAR T-cell case we may estimate treatment success probability from Eq. S53 as a function of Eq. S55 and $P_l(m_0 < m < M)$, given by Eq. S51, as

$$\begin{aligned} P_T &= P_{\mu^c} \cdot \big(P_{e,\mu} + P_{e,\mu^c} + P_{e^c,\mu}\big) \\ &= \big(1 - P_{e^c,\mu}(m_{mrd}; m_{mrd})\big)\big(1 - P_l(m_0 \leq m \leq M)\big). \end{aligned} \tag{S56}$$

CAR T-cell treatment benefit is illustrated under a variety of immune parameters in Fig. 6. We observe that CAR T-cell therapy is predicted to be largely beneficial for both immune-competent and immune-compromised patients, consistent with the fact that CAR T-cell therapy functions independently from the status of the native T-cell repertoire. CAR T-cell therapy is predicted to be less effective against faster-growth threats, as the prolonged death phase allows a greater change of CAR T-cell evader arrival.

S7.3 Autologous neoantigen vaccines

Autologous neoantigen vaccines are another immunotherapeutic strategy which relies on the delivery of (possibly multiple) tumor neoantignes to the cell in order to augment or enhance the effect of neoantigen-specific CD8+ T-cells [18]. Contrasting their reduced efficacy in tumors with lower mutation rates [15], neoantigen vaccines have been successful in augmenting cancer remission in highly mutagenic tumors, such as melanoma, where the neoantigen burden is significant [19–21]. In our framework, successful immune priming occurs when a large amount of vaccine-delivered antigen suddenly becomes available to activate T-cells and serves to effectively reduce the detection threshold R. For simplicity we assume that a sufficient level of tumor antigens are present so that $R = 0$ and any cancer size can be targeted.

In contrast to the previous case, vaccine therapy cannot rescue a patient with immune-evasive cells and so in our model this strategy may only be successful if there is an absence of type-2 cells both before and after treatment (i.e. on E_{μ^c}). On the therapeutically relevant event, E_{e,μ^c}, subsequent treatment success occurs only if the threat neither escapes nor acquires an immune-evasive phenotype E_{e^c,μ^c}. This relevant probability, denoted by $P_l(m_{mrd} \leq m \leq M; m_{mrd})$, is related to the probability of adaptive threat loss given by Eq. S51 modified to account for the fact that the process starts at $X(T_D+) = m_{mrd}$. It is given by

$$P_l(m_{mrd} \leq m \leq M; m_{mrd}) \equiv 1 - \big(P_{e^c,\mu}(m_{mrd} \leq m \leq M; m_{mrd}) + P_e\big) \tag{S57}$$

with $P_e = p_e(M; m_{mrd})$, and

$$P_{e^c,\mu}(m_{mrd} \leq m \leq M; m_{mrd}) \equiv \sum_{m=m_{mrd}}^{M} P_{e^c,\mu}(m; m_{mrd}) \cdot p_r(m; m_{mrd}). \tag{S58}$$

In summary, conditional treatment success probabilities become:

$$\mathbb{P}\big(E \mid E_{e,\mu^c}\big) = P_l\big(m_{mrd} \leq m \leq M; m_{mrd}\big); \tag{S59}$$

$$\mathbb{P}\big(E \mid E_{e,\mu}\big) \ = 0; \tag{S60}$$

$$\mathbb{P}\big(E \mid E_{e^c,\mu}\big) = 0. \tag{S61}$$

In Eq. S60 we have implicitly assumed that the post-treatment subset of m_{mrd} cells from the original population of size M always contains an evasive sub-clone if at least one type-2 cell is present at detection. A more detailed analysis would estimate the sub-population size distribution of type-2 cells at overall size M and quantify their presence or absence following ablation; for now, we proceed with this lower-estimate on efficacy. Thus, treatment success probability depends exclusively on the middle term in Eq. S53. The final required calculation measures escape probability without acquired immune evasion (P_{e,μ^c}) under adaptive, growth limited detection as follows:

$$\begin{aligned} P_{e,\mu^c} &= \mathbb{P}\big(E_{\mu^c} \mid E_e\big)\mathbb{P}\big(E_e\big) \\ &= (1-\mu)^M \cdot p_e\big(M; m_0\big) \\ &\approx (1-\mu)^M \left[I_{[m_0 > M]} + p_b \left(\frac{m_0}{M} \right)^{k/r} \cdot I_{m_0 \leq M} \right], \end{aligned} \tag{S62}$$

where the indicator function has been used to guarantee escape if $m_0(r) > M$. Therefore,

$$P_T = P_l(m_{mrd} \leq m \leq M; m_{mrd}) P_{e,\mu^c}. \tag{S63}$$

Vaccine treatment benefit is illustrated alongside CAR T therapy in Fig. 6. The effect of neoantigen vaccines is predicted to be most robust against slower growing threats that would normally escape immune detection via slow-growth.

References

[1] G. Bocharov, B. Ludewig, A. Bertoletti, P. Klenerman, T. Junt, P. Krebs, C. Fraser, R. M. Anderson, and T. Luzyanina, "Underwhelming the Immune Response : Effect of Slow Virus Growth on CD8 + T-Lymphocyte Responses," Journal of virology, vol. 78, no. 5, pp. 2247–2254, 2004.

[2] R. E. Lyons, R. McLeod, and C. W. Roberts, "Toxoplasma gondii tachyzoite–bradyzoite interconversion," Trends in parasitology, vol. 18, no. 5, pp. 198–201, 2002.

[3] K. Naylor, G. Li, A. N. Vallejo, W.-W. Lee, K. Koetz, E. Bryl, J. Witkowski, J. Fulbright, C. M. Weyand, and J. J. Goronzy, "The influence of age on t cell generation and tcr diversity," The Journal of Immunology, vol. 174, no. 11, pp. 7446–7452, 2005.

[4] J. T. George, D. A. Kessler, and H. Levine, "Effects of thymic selection on t cell recognition of foreign and tumor antigenic peptides," Proceedings of the National Academy of Sciences, p. 201708573, 2017.

[5] J. Pido-Lopez, N. Imami, and R. Aspinall, "Both age and gender affect thymic output : more recent thymic migrants in females than males as they age," Clin Exp Immunol, pp. 409–413, 2001.

[6] P. Armitage and R. Doll, "The age distribution of cancer and a multi-stage theory of carcinogenesis," British journal of cancer, vol. 8, no. 1, p. 1, 1954.

[7] B. Stransky and S. Desouza, "Modeling tumor evolutionary dynamics," Frontiers in physiology, vol. 3, p. 480, 2013.

[8] G. A. Holländer, W. Krenger, and B. R. Blazar, "Emerging strategies to boost thymic function," Current opinion in pharmacology, vol. 10, no. 4, pp. 443–453, 2010.

[9] J. Offman, G. Opelz, B. Doehler, D. Cummins, O. Halil, N. R. Banner, M. M. Burke, D. Sullivan, P. Macpherson, and P. Karran, "Defective dna mismatch repair in acute myeloid leukemia/myelodysplastic syndrome after organ transplantation," Blood, vol. 104, no. 3, pp. 822–828, 2004.

[10] M. Sadelain, I. Rivière, and S. Riddell, "Therapeutic T cell engineering," Nature Publishing Group, vol. 545, no. 7655, pp. 423–431, 2017.

[11] D. Abate-Daga and M. L. Davila, "CAR models: Next-generation CAR modifications for enhanced T-cell function," Molecular Therapy - Oncolytics, vol. 3, no. February, p. 16014, 2016.

[12] H. Almåsbak, T. Aarvak, and M. C. Vemuri, "CAR T Cell Therapy : A Game Changer in Cancer Treatment," Journal of Immunology Research, vol. 2016, no. signal 1, 2016.

[13] S. Yu, A. Li, Q. Liu, T. Li, X. Yuan, X. Han, and K. Wu, "Chimeric antigen receptor t cells: a novel therapy for solid tumors," Journal of hematology & oncology, vol. 10, no. 1, p. 78, 2017.

[14] X. Wang and I. Rivière, "Clinical manufacturing of CAR T cells: Foundation of a promising therapy," Molecular Therapy - Oncolytics, vol. 3, no. February, pp. 1–7, 2016.

[15] S. D. Martin, S. D. Brown, D. A. Wick, J. S. Nielsen, D. R. Kroeger, K. Twumasi-Boateng, R. A. Holt, and B. H. Nelson, "Low mutation burden in ovarian cancer may limit the utility of neoantigen-targeted vaccines," PLoS ONE, vol. 11, no. 5, p. e0155189, 2016.

[16] C. E. Brown and P. S. Adusumilli, "Next frontiers in CAR T-cell therapy," Molecular Therapy - Oncolytics, vol. 3, p. 16028, 2016.

[17] K. Newick, E. Moon, and S. M. Albelda, "Chimeric antigen receptor T-cell therapy for solid tumors," Molecular Therapy - Oncolytics, vol. 3, no. October 2015, p. 16006, 2016.

[18] E. F. Fritsch, N. Hacohen, and C. J. Wu, "Personal neoantigen cancer vaccines: the momentum builds," OncoImmunology, 2014.

[19] P. A. Ott, Z. Hu, D. B. Keskin, S. A. Shukla, J. Sun, D. J. Bozym, W. Zhang, A. Luoma, A. Giobbie-Hurder, L. Peter, C. Chen, O. Olive, T. A. Carter, S. Li, D. J. Lieb, T. Eisenhaure, E. Gjini, J. Stevens, W. J. Lane, I. Javeri, K. Nellaiappan, A. M. Salazar, H. Daley, M. Seaman, E. I. Buchbinder, C. H. Yoon, M. Harden, N. Lennon, S. Gabriel, S. J. Rodig, D. H. Barouch, J. C. Aster, G. Getz, K. Wucherpfennig, D. Neuberg, J. Ritz, E. S. Lander, E. F. Fritsch, N. Hacohen, and C. J. Wu, "An immunogenic personal neoantigen vaccine for patients with melanoma," Nature, vol. 547, pp. 217–221, 2017.

[20] M. D. Hellmann and A. Snyder, "Making It Personal: Neoantigen Vaccines in Metastatic Melanoma," 2017.

[21] U. Sahin, E. Derhovanessian, M. Miller, B.-p. Kloke, P. Simon, M. Löwer, V. Bukur, A. D. Tadmor, U. Luxemburger, B. Schrörs, T. Omokoko, M. Vormehr, C. Albrecht, A. Paruzynski, A. N. Kuhn, J. Buck, S. Heesch, K. H. Schreeb, F. Müller, I. Ortseifer, I. Vogler, E. Godehardt, S. Attig, R. Rae, A. Breitkreuz, C. Tolliver, M. Suchan, G. Martic, A. Hohberger, P. Sorn, J. Diekmann, J. Ciesla, O. Waksmann, A.-k. Brück, M. Witt, M. Zillgen, A. Rothermel, B. Kasemann, D. Langer, S. Bolte, M. Diken, S. Kreiter, R. Nemecek, C. Gebhardt, S. Grabbe, C. Höller, J. Utikal, C. Huber, C. Loquai, and Ö. Türeci, "poly-specific therapeutic immunity against cancer," Nature Publishing Group, vol. 547, no. 7662, pp. 222–226, 2017.